GLOBAL BIOGEOCHEMICAL CYCLES, VOL. 3, NO. 3, PAGES 241-265, SEPTEMBER 1989

CONTINENTAL SCALE MODELS OF WATER BALANCE AND FLUVIAL TRANSPORT: AN APPLICATION TO SOUTH AMERICA

Charles J. Vörösmarty, Berrien Moore III,
Annette L. Grace, and M. Patricia Gildea

Institute for the Study of Earth, Oceans
and Space, University of New Hampshire,
Durham

Jerry M. Melillo, Bruce J. Peterson,
Edward B. Rastetter, and Paul A. Steudler

Ecosystems Center, Marine Biological
Laboratory, Woods Hole, Massachusetts

Abstract. A coupled water balance and water transport model (WBM / WTM) was constructed as part of a larger study of global biogeochemistry. The WBM / WTM provides critical hydrologic information to models of terrestrial primary production, organic matter decay, riverine nutrient flux and trace gas exchanges with the troposphere. Specifically, it creates high-resolution data sets for monthly soil moisture, evapotranspiration, runoff, river discharge and floodplain inundation. As a first step toward eventual global coverage, the WBM / WTM was applied to South America, represented by more than 5700 1/2° (latitude / longitude) grid cells. The WBM transforms spatially complex data on long-term climate, vegetation, soils and topography into predictions of soil moisture (SM), evapotranspiration (ET) and runoff (RO). For South America, field capacity in soils ranged from 27 to 582 mm of water, and computed values for mean annual SM, ET and RO were 284 mm, 1059 mm/yr and 619 mm/yr, respectively. There were large differences regionally and over the year. The transport model uses WBM-derived runoff, information on fluvial topology, linear transfer through river channels and a simple representation of floodplain inundation to generate monthly discharge estimates for any cell within a simulated catchment. The WTM successfully determined the timing and magnitude of discharge at selected locations within the Amazon / Tocantins basin. It also demonstrated the importance of floodplain inundation in defining flow regime on the mainstem Amazon. Estimated mean annual discharge was 207,000 m^3/s for the Amazon River and 17,000 m^3/s for the Tocantins. In these basins, 45% of the incident precipitation emerges as river flow; 55% is lost to ET. The model described in this paper will be expanded to include the dynamics of carbon, major nutrients and sediments. It will serve as a semimechanistic tool to quantify the transport of materials from the landscape to the world's oceans. Such a capability becomes increasingly important as we seek to understand the impacts of climate and land use change on major river systems of the globe.

Paper number 89GB01529.
0886-6236/89/89GB-01529$10.00

INTRODUCTION

The terrestrial water cycle is a key component of the Earth's climate and biogeochemistry. Associated with this cycle is a continuous exchange of water, energy and materials through the atmosphere, the landscape and inland aquatic ecosystems. Water also activates and is influenced by a myriad of biospheric processes including plant production, organic matter decay and gas exchange between terrestrial ecosystems and the lower troposphere. The availability of freshwater resources has obvious effects on human society as well. The hydrologic cycle is clearly important at local, regional, and global scales.

The impetus for studying the global water cycle has been articulated many times [International Geosphere-Biosphere Program (IGBP), 1988; National Aeronautics and Space Administration (NASA) / Earth System Sciences Committee (ESSC), 1988; Eagleson, 1986]. Of fundamental concern is the growing body of evidence implicating human activity as a major factor in global change. With the advent of requisite instrumentation and data base management capabilities, the scientific community is rapidly approaching a situation in which the hydrologic cycle can be carefully monitored over vast regions. There is, however, a decided need for scientific tools which can aid researchers in analyzing the observational data sets to better understand the role of water in geosphere-biosphere dynamics.

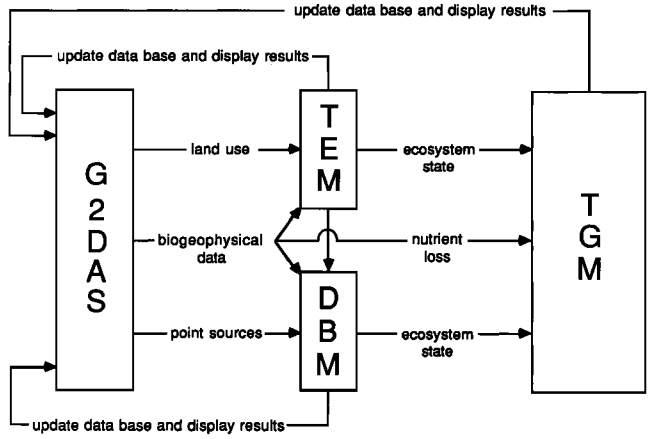

Fig. 1. Modeling efforts in the study of global biogeochemical cycles. Information is organized in a global geographically referenced data analysis system (G2DAS) which supports the data needs of a terrestrial ecosystem model (TEM), a drainage basin model (DBM), and a trace gas model (TGM), each organized at the 1/2° x 1/2° (latitude x longitude) spatial scale. This paper describes the hydrologic components of DBM.

The overall goal of our research is to study major biogeochemical cycles at the global scale. We seek to quantify rates of nutrient and carbon flux in terrestrial ecosystems and their exchanges among the landscape, inland aquatic ecosystems and the atmosphere [Moore et al., 1989]. An important research activity is the development of models to aid in analyzing these phenomena (Figure 1).

This paper describes the hydrologic component of a larger drainage basin model (DBM) which treats both water and constituent flux. The hydrologic component consists of a water balance model (WBM) and a water transport model (WTM) (Figure 2). The spatial domain of each model is organized as a set of geographically referenced grid cells at the 1/2° x 1/2° (latitude x longitude) scale. The WBM operates on independent grid cells and uses biogeophysical information to predict monthly soil moisture, evapotranspiration and runoff. The water balance calculations are linked to the terrestrial ecosystem model (TEM) and trace gas model (TGM) shown in Figure 1 through soil moisture and evapotranspiration. The WTM links single grid cells to define an integrated drainage basin topology. Discharge estimates are then made by routing WBM-derived runoff through simulated catchments.

Our work complements other regional and global studies of surface hydrology and material transport [Richey and Ribeiro, 1987; Vorosmarty et al., 1986; Elder, 1985; Milliman and Meade, 1983; Stallard and Edmond, 1983; Meybeck, 1982; Giannessi et al., 1981; United Nations, 1981; Brunskill et al., 1975]. The methodology builds on earlier work using gridded climate and hydrologic models at a variety of spatial scales by Wiltshire et al. [1986], Willmott et al. [1985a], Schmidt [1981] and Cluis et al. [1979].

The initial focus is South America, with particular emphasis on Amazonia. We choose this area for several reasons. Water flux is a dominant yet often poorly measured feature over much of the continent and refined estimates will be useful to a variety of scientific investigations. These include studies of biomass distribution and productivity, the biogeochemistry of large tropical rivers (for example, Carbon in the Amazon River Experiment (CAMREX) (Brazilian-U.S. Consortium, J. Richey) and Projecto Orinoco-Apure (POA) (Ministerio del Ambiente y de los Recursos Naturales Renovables, Venezuela, A. Mejia)) and floodplain inundation as a mediator of trace gas exchange [Quay et al., 1988]. Although broad regions of the Amazonian rainforest remain undisturbed, they are increasingly subject to disruption [Fearnside, 1986]. Since the recycling of precipitable water through evapotranspiration is an important characteristic of basin hydrology [Salati and Vose, 1984], documenting its recent status will provide an important benchmark against which future anthropogenic disturbance and climate change can be assessed.

MODEL DEVELOPMENT

To address scientific issues at the continental scale, terrestrial hydrologic models must characterize the dispersed nature of climate and hydrology over space and time while avoiding needless complexity. Although the science of hydrology, and hydrologic modeling in particular, is now quite sophisticated [Burges, 1986; Singh, 1982], a continental-scale model requires prudent simplification [Dooge, 1986]. In the current context, simplification is required not only for reasonable computing time but also for developing a generic form applicable to a broad spectrum of systems across the globe. The model must also exploit the current generation of global data sets available in point, polygonal or gridded format. To facilitate global coverage the model requires a minimal number of parameters for calibration.

Water Balance Model: Structure

The WBM simulates grid cell level hydrology associated with long-term climate (Figure 3). Inputs to the WBM include global- or continental-scale data sets covering precipitation, temperature, potential evapotranspiration, vegetation, soils and elevation. The WBM then predicts soil

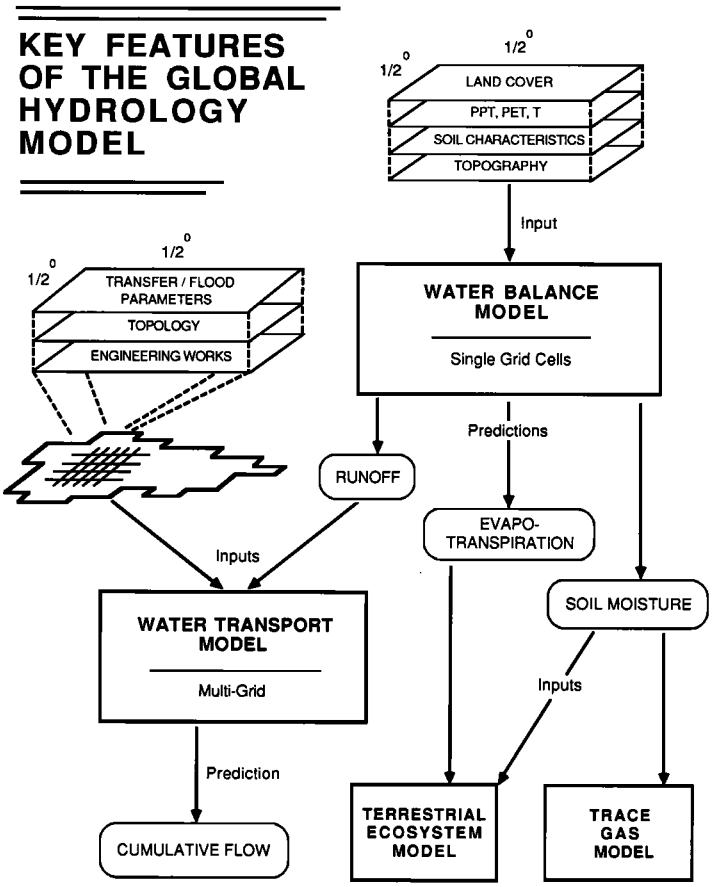

Fig. 2. Structure of the global hydrologic model, showing the relationship between water balance and water transport models and a set of gridded data sets. The hydrologic model links to TEM and TGM through calculated evapotranspiration and soil moisture.

moisture (SM), evapotranspiration (ET) and runoff (RO) for each 1/2° grid cell in the simulated region. In the current study, independent water balance predictions are made for more than 5700 cells representing South America. The WBM component relies on techniques developed by Thornthwaite and Mather [1957] and subsequently modified as part of the current work.

The climatic variables are determined from long-term monthly averages for precipitation (PPT), temperature (T), and potential evapotranspiration (PET). In any month, rain and snow can occur simultaneously. The model is deterministic and employs a monthly time step. A dynamic steady state is achieved by applying monthly PPT, T and PET repeatedly over the year until the soil moisture, ET, runoff and snowmelt calculations for each successive twelve-month period converge to within an acceptable margin of difference (0.01%).

Soil moisture is determined from interactions among rainfall, snowmelt recharge and PET. During wet months (rain plus snowmelt in excess of PET), soil moisture can increase up to a maximum field capacity determined by soil texture and rooting depth. During dry periods (available water exceeded by PET), soil moisture becomes a function of potential water loss. Thus

$$dSM/dt = (P_r + R_s - PET) \qquad P_r + R_s \geq PET,\ SM < FC \quad (1a)$$

$$dSM/dt = 0 \qquad P_r + R_s \geq PET,\ SM = FC \quad (1b)$$

$$dSM/dt = -a\,SM\,(PET - [P_r + R_s]) \qquad P_r + R_s < PET \quad (1c)$$

where SM is soil moisture (millimeters), P_r is precipitation as rainfall (millimeters per month), R_s is snowmelt recharge (millimeters per month), PET is potential ET (millimeters per month), FC is soil field capacity (millimeters) and a is the slope of the moisture retention function described below. Calculations commence at the end of the wet season when it is assumed the soil is at field capacity. Soil water stocks are then depleted during the dry season in accordance with the moisture retention function. For each wet month, soil moisture is determined by incrementing antecedent values by the excess of available water over PET. This recharge may or

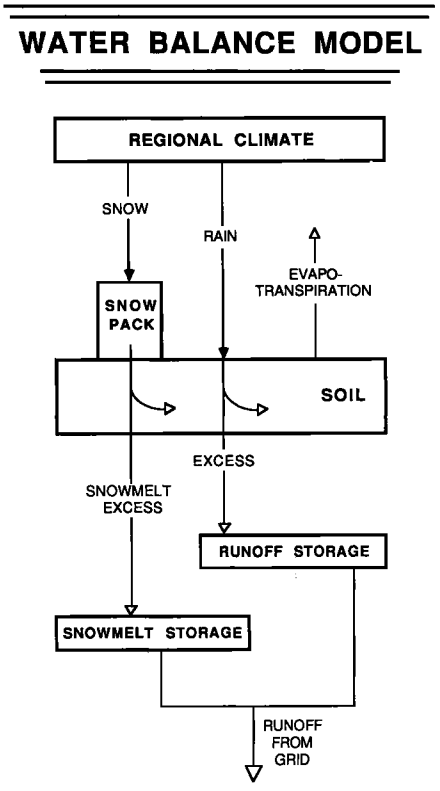

Fig. 3. The water balance model showing pools and water transfers. Through a retention function for soil water, the model transforms precipitation and potential evapotranspiration into soil moisture, evapotranspiration and runoff. Closed triangles represent inputs; open triangles are flux determinations made by the model.

may not be sufficient to bring the soil to field capacity at the end of the subsequent wet season.

As a soil dries it becomes increasingly difficult to remove moisture against increasing pore tension. For a particular soil, there is a linear relationship between *log* SM and Σ [PET - ($P_r + R_s$)], summed from the start of the dry season to the current month. The original tables offered by Thornthwaite and Mather [1957] treated eleven field capacities in metric units. To calculate dSM / dt through (1c) for intermediate field capacities, the WBM defines a slope to the retention function:

$$a = ln\,(FC) / (1.1282\ FC)^{1.2756} \qquad (2)$$

The numerator represents soil moisture (millimeters) with no net drying. The denominator is the accumulated potential water loss (Σ [PET - ($P_r + R_s$)]) in millimeters at SM = 1.0 mm. With a determined the model can calculate dSM / dt as a function of soil dryness and update SM. Calculations for SM are similar to those used by Pastor and Post [1984].

The WBM calculates soil moisture to a maximum defined by the field capacity for a particular soil (i.e., moisture held in the soil drained by gravity). It makes no prediction of the degree of waterlogging beyond this capacity. Such a determination would require assignment of percolation rates to each soil type as well as a statistical distribution of rainfall duration and intensity over each month. Furthermore, the hydrology simulated in the current version of WBM is driven by pluvial processes alone; floodplain inundation is not explicitly considered.

Once soil moisture is determined evapotranspiration is calculated. Following Thornthwaite and Mather, ET is set equal to PET in wet months, when $P_r + R_s \geq$ PET. During such times it is assumed that precipitation and any available snowmelt are in sufficient abundance to satisfy all potential water demands of the resident vegetation. During dry seasons ($P_r + R_s <$ PET) the monthly average ET (in millimeters) is modified downward from its potential. The relevant equations are

$$ET = PET \qquad P_r + R_s \geq PET \qquad (3a)$$

$$ET = P_r + R_s - dSM / dt \qquad P_r + R_s < PET \qquad (3b)$$

The WBM calculates runoff based on the availability of soil moisture. Whenever field capacity is attained, excess water is transferred to subsurface runoff pools for rain and snowmelt. From these storage pools, RO is generated as a linear function of the existing pool size. The transfer coefficients are set according to Thornthwaite and Mather [1957]. There is no contribution to the runoff storage pools when a moisture deficit exists in relation to field capacity; any available water recharges the soil. For rainfall runoff we get

$$RO_r = 0.5\,[\,D_r + p\,(P_r + R_s - PET)] \qquad SM = FC\,,\ P_r + R_s \geq PET \qquad (4a)$$

$$RO_r = 0.5\,D_r \qquad SM < FC \text{ or } P_r + R_s < PET \qquad (4b)$$

where RO_r is rainfall-derived runoff (millimeters per month), D_r is rainfall-derived detention (storage) pool (millimeters) and p is the proportion of surplus water attributable to rain (P_r / [$P_r + R_s$]).

Snowpack accumulates whenever mean monthly temperature is below -1.0°C. Snowmelt occurs at or above -1.0°C. Using snowmelt relationships developed by Willmott et al. [1985a] and water budgets developed for fourteen ecosystem study sites [Univ. of New Hampshire / Marine Biological Laboratory, 1989], we developed a simple representation of snowpack behavior. At elevations of 500 m or less, the model removes the entire snowpack (plus any new snow) by the end of the first month of snowmelt. At elevations above 500 m, the melting process requires two months with half of the first month's snowpack retained until the second. Snowmelt is used first to recharge any soil moisture deficit. Any excess is then passed to a snowmelt storage pool for eventual runoff. By Thornthwaite and Mather [1957], sites at elevations of 500 m or less will lose 10% of this pool in the first month of snowmelt. In subsequent months, these sites will lose 50% per month. At higher elevations, sites will lose 10% in the

first month, followed by 25% in the second month and 50% thereafter. For snowmelt at or below 500 m elevation we therefore have

$$RO_s = 0.1\ (D_s + PK_s) \qquad \text{month} = 1 \text{ of } T \geq -1.0\ ^\circ C \quad (5a)$$

$$RO_s = 0.5\ D_s \qquad \text{month} > 1 \text{ of } T \geq -1.0\ ^\circ C \quad (5b)$$

where RO_s is snowmelt-derived runoff (millimeters per month), D_s is snowmelt-derived detention (storage) pool (millimeters) and PK_s is snowpack (millimeters of water) available after any required soil moisture recharge. For snowmelt above 500 m elevation we get

$$RO_s = 0.1\ (D_s + 0.5\ PK_s) \qquad \text{month} = 1 \text{ of } T \geq -1.0\ ^\circ C \quad (6a)$$

$$RO_s = 0.25\ (D_s + PK_s) \qquad \text{month} = 2 \text{ of } T \geq -1.0\ ^\circ C \quad (6b)$$

$$RO_s = 0.5\ D_s \qquad \text{month} > 2 \text{ of } T \geq -1.0\ ^\circ C \quad (6c)$$

These equations are combined with the rainfall-derived runoff to yield the aggregate runoff (RO) from each grid cell. This RO is used as an input to the WTM.

Water Balance Model: Required Data

The WBM requires a number of geographically referenced data sets which cover climatology, vegetation, soil texture and topography. This section identifies these data sources and the steps taken to prepare them for eventual use in the WBM.

Precipitation data were taken from the UNESCO *Atlas of World Water Balance* [Korzoun et al., 1977]. Isohyets of mean total precipitation (millimeters per year) were digitized and subsequently gridded to the 1/2° scale using ARC / INFO [Environmental Systems Research Institute Inc., Redlands, California] Geographical Information System (GIS) software. Monthly rain or snow was determined from site-specific histograms (showing percent annual precipitation) and two-dimensional interpolation [Akima, 1978]. The potential ET data set, also from Korzoun et al. [1977], was developed in the same manner. The PET entries are based on air temperature, radiation balance and moisture content of evaporating surfaces. Interception losses are not explicitly treated but are included as part of the PET estimates. At the continental scale, PPT and PET amount to 1679 and 1336 mm/yr.

Snowmelt determinations required additional data sets for surface air temperature and elevation. Mean monthly temperature data were obtained from Willmott and Rowe [1986], recoded into 1/2° grid cells. We obtained elevation above mean sea level (msl) in 30-m vertical increments from a digital data set available through the National Center for Atmospheric Research (NCAR) / NAVY [1984]. The original data set was organized at the 10-min scale. We aggregated the "modal" elevation data into 1/2° grid cells.

Field capacity for each grid cell was determined as a function of soil texture and vegetation (Table 1). Six soil texture classes were considered in conjunction with two broad categories of vegetative cover. First, we assigned a characteristic field capacity, as percent of total soil volume, to the six texture classes using data from Saxton et al. [1986] representing soil moisture at 30-kPa water potential. We then established rooting depths for the various combinations of soil texture and vegetation using the assignment scheme given by

TABLE 1. Relationships Linking Vegetation Class, Soil Texture, Rooting Depth and Moisture Capacities of Soil

Vegetation[a]	Sand	Sandy Loam	Silt Loam	Clay Loam	Clay	Lithosol
			Root Depth, m			
Forest	2.5	2.0	2.0	1.6	1.2	0.1
Grassland and shrubland	1.0	1.0	1.3	1.0	0.7	0.1
	Field Capacity[b], and Available Water Capacity (in Parentheses)[c], mm of water					
Forest	353.0 (196.0)	400.0 (218.0)	546.0 (282.0)	563.0 (243.0)	582.0 (153.0)	27.0 (14.0)
Grassland and shrubland	141.0 (78.0)	200.0 (109.0)	355.0 (183.0)	352.0 (152.0)	340.0 (89.0)	27.0 (14.0)

[a]WBM forests were assigned rooting depths for "mature forest" given by Thornthwaite and Mather [1957], WBM grasslands and shrublands were given rooting depths for "deep rooted crops."

[b]The field capacity values in mm were determined using the following values representing field capacity as a percentage of total soil volume: 14.1% (sand), 20.0 (sandy loam), 27.3 (silt loam), 35.2 (clay loam), 48.5 (clay). Field capacity was taken as moisture content at 30-kPa water potential. These values were taken from Saxton et al. [1986]. Lithosols were assigned a value of 27.3% and were assumed to have a rooting depth of 0.1 m for all vegetation classes.

[c]The available water capacities (field capacity minus wilting point) in millimeters were determined using the following values representing wilting point as a percentage of total soil volume: 6.3% (sand), 9.1 (sandy loam), 13.2 (silt loam), 20.0 (clay loam), 35.8 (clay). Wilting point was taken as moisture content at 1500-kPa water potential. These values were taken from Saxton et al. [1986]. Lithosols were assigned a value of 13.2% and were assumed to have a rooting depth of 0.1 m for all vegetation classes.

TABLE 2. Distribution of South American Ecosystems

Ecosystem	Area, 10^6 km^2
Forest	
Tropical evergreen forests	6.778
Tropical and subtropical drought-deciduous forests	1.488
Tropical and subtropical semi-deciduous broad-leaved forests	0.210
Subtropical evergreen forests	0.182
Temperate evergreen broad-leaved forests	0.017
Temperate mixed forests	0.014
Drought-deciduous woodlands	0.012
Total forest	8.700
Shrubland	
Xeric forests and woodlands	2.050
Xeric shrublands and scrub	1.338
Total shrubland	3.388
Grassland	
Savannas,10-40% tree cover	1.909
Short grasslands, meadows, tropical alpine vegetation	1.115
Savannas, <10% tree cover	0.952
Tall grassland	0.458
Shrub savanna	0.309
Total grassland	4.743
Grand total	16.832

The ecosystem types listed were obtained from Matthews [1983] and classified into broad categories of vegetation in order to utilize information in Table 1 to distribute field and available water capacities over space. Areas given are corrected for latitude. Only those areas for which actual WBM calculations were made are tabulated. Totals may not add due to rounding.

Thornthwaite and Mather [1957]. The product of field capacity percentage and rooting depth defined field capacity in millimeters. Except for lithosols (very rocky soils), specific values for the resulting FCs were therefore vegetation and texture dependent. Eleven potential field capacities were generated, from 27 to 582 mm of water.

A similar set of calculations was made for available water capacity (AWC), defined as field capacity minus wilting point. Because of its dependence on vegetation and soil characteristics, AWC also showed a broad numerical range, from 14 to 282 mm (Table 1). These values represent an alternative to the use of a spatially uniform AWC field of 150 mm, evident in recent global climate modeling studies [Kellogg and Zhao, 1987].

The values presented in Table 1 together with a series of geographically referenced data sets were used to determine the distribution of FC and AWC across the continent. Soil texture for South America was derived from gridded 1:5,000,000 scale soil maps [Food and Agriculture Organization / Complex Systems Research Center (FAO / CSRC), 1974]. (The following FAO classifications were assigned to the various texture classes shown in Table 1: "coarse" was assigned to sand, "medium" to silt loam, "fine" to clay, "coarse + medium" to sandy loam, "coarse + fine" to silt loam, "medium + fine" to clay loam, and "coarse + medium + fine" to silt loam.) Vegetative cover was from Matthews [1983], converted to 1/2° resolution. Table 2 lists 14 broad ecosystem types and their associated areas. The dominant vegetation is forest (> 50% of all area) and in particular the tropical evergreen forest. Grasslands and savannas comprise approximately 30% of the continental landmass. Shrubland accounts for the remaining 20%. Ten field capacity classes are present ranging from 27 to 582 mm with an area-weighted mean of 394 mm. A map of the resulting field capacities is shown in Plate 1. The distribution of available water capacity is shown in Plate 2. The ten AWC classes range from 14 to 282 mm. The area-weighted mean for South America is 144 mm.

The spatial patterns of FC and AWC correlate well with the distribution of vegetation. Thus, forested areas with high capacities contrast sharply against lower-biomass regions having smaller values. Another dominant feature is the level of detail afforded by the 1/2° scale, a product of the original soil and vegetation data sets. These maps represent the most spatially resolved estimates of FC and AWC currently available for South America.

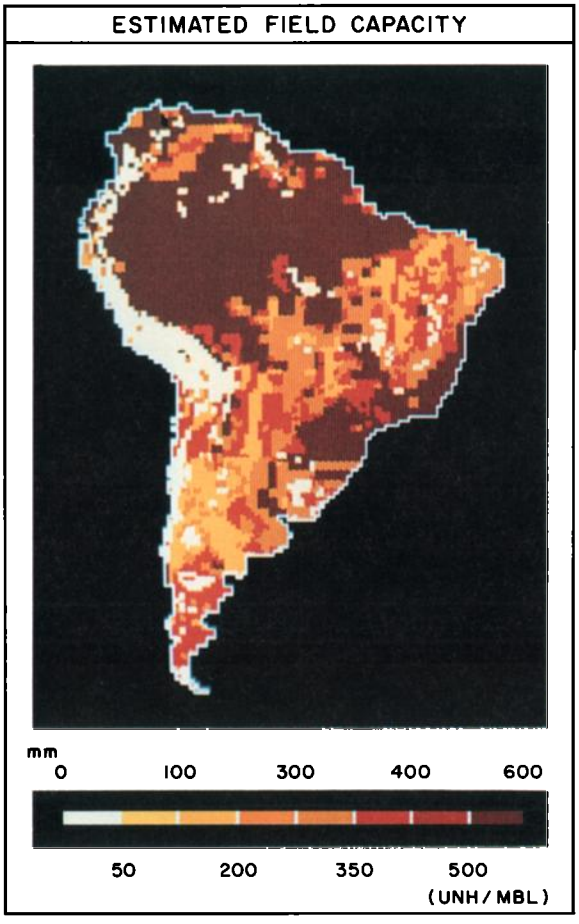

Plate 1. Field capacities used by the water balance model at 1/2° spatial resolution. The capacities were generated using Table 1 and geographically specific information on soils and vegetation. The areas represented by particular field capacities are 27 mm (1.9 x 10^6 km^2), 141 (1.7 x 10^6), 200 (0.003 x 10^6), 340 (2.8 x 10^6), 352-355 (2.6 x 10^6), 546 (2.5 x 10^6), 563 (0.4 x 10^6), and 582 (4.9 x 10^6).

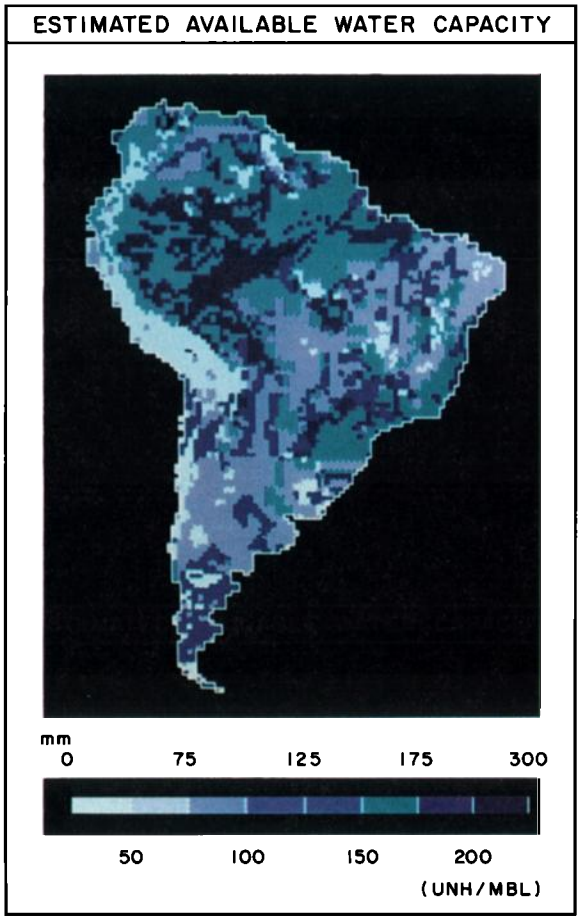

Plate 2. Available water capacity (field capacity minus wilting point) computed by the water balance model at 1/2° spatial resolution. The values were generated using Table 1 and geographically specific information on soils and vegetation. The areas represented by particular available water capacities are 14 mm (1.9 x 10^6 km^2), 78 (1.7 x 10^6), 89 (2.8 x 10^6), 109 (0.003 x 10^6), 152 (0.4 x 10^6), 153 (4.9 x 10^6), 183 (1.9 x 10^6), 196 (0.3 x 10^6), 243 (0.4 x 10^6), and 282 (2.5 x 10^6). The mean area-weighted average is 144 mm.

Water Transport Model: Structure and Parameterization

The water transport model is a multigrid, dynamic model which computes discharge through each cell within a simulated drainage basin (Figure 2). It combines runoff produced by WBM with information on network topology, fluvial transfer rates and the timing and extent of floodplain inundation. Discharge is predicted as a monthly mean. Because WBM-generated runoff drives the transport model, predicted discharges represent long-term climatic averages. Initial application of this model has been to the Amazon / Tocantins river system which represents nearly one fifth of the world's freshwater discharge. The simulated Amazon Basin comprises 1936 grid cells (5.92 x 10^6 km^2). The Tocantins River adds another 315 cells (0.96 x 10^6 km^2).

Network topology was determined manually from a series of 1·1,000,000 Operational Navigation Charts [Defense Mapping Agency Aerospace Center (DMAAC), 1980, 1981, 1982, 1983, 1984, 1986] covering the Amazon / Tocantins system. For each 1/2° cell, a predominant direction of flow was determined by examining the discernible network of rivers and streams. With large rivers this afforded an unambiguous indicator of directionality. In grid cells draining small areas, a predominant stream was sometimes absent. In these cases we relied on topographic features and elevational data reported on the DMAAC maps. Flow direction was therefore predicted less accurately for small rivers than for larger rivers. This effect was common in subcatchments of four or fewer grid cells (30% or more of such grid cells had less reliable directionality). A four-cell basin near the equator is approximately 12,000 km^2, an area similar to that of a sixth-order stream [Leopold et al., 1964]. This represents the theoretical limit of WTM spatial resolution using a 1/2° grid structure

Channel flow in the WTM is represented by a linear reservoir model [Huggins and Burney, 1982]. Each grid is considered a storage pool with a characteristic residence time (t). We assign a standard transfer coefficient, K (t^{-1}), to all cells and then modify this parameter based on geometric considerations. The standard is associated with rivers draining grid cells on the N-S or E-W axis. The K value is then lengthened or shortened depending on the geometry of influent and effluent streams. For example, a cell receiving influent from the southwest and with an exit at its northeast corner would have the standard K value multiplied by 0.7 to accommodate a longer residence in the grid cell. In the case of multiple tributaries, the residence time is weighted by mean annual flow. For grid cells lacking upstream inputs, the residence time is halved.

The WTM also predicts floodplain inundation independently of any WBM calculations. We have chosen flood parameters in WTM that have clear physical analogues. Floodplain exchanges take place whenever the monthly discharge exiting a grid cell exceeds a specified fraction of long-term mean annual flow. Above this fraction and with increasing discharge, inundation is simulated by apportioning the potential net increase in grid cell water storage between the channel itself and its associated floodplain. Floodplain storage increases until the time derivative of grid cell storage becomes negative. During flood recession, the potential net decrease in grid cell storage is accounted for by changes in channel and floodplain storage using the same ratios as for rising waters. These calculations attenuate the amplitude of rising flood waves and augment downstream discharge during periods of falling stage. For a single grid cell, the resulting flow and continuity equations are

$$dS_c / dt = (\sum_1^n Q_u) - Q_d + Q_g + Q_f \quad (7a)$$

$$dS_f / dt = - Q_f \quad (7b)$$

$$Q_d = K S_c \quad (7c)$$

$$Q_g = A (RO_r + RO_s) / 1000. \quad (7d)$$

$$Q_f = -r_f [(\sum_1^n Q_u) - Q_d + Q_g] \qquad Q_d \geq c_f Q_{dma} \quad (7e)$$

$$Q_f = 0 \qquad Q_d < c_f Q_{dma} \quad (7f)$$

where S_c is channel storage in a grid cell during a month (cubic meters), S_f is floodplain storage (cubic meters), K is the downstream transfer coefficient (month^{-1}), A is the area of the grid (square meters), n is the number of donor grid cells, Q_u is monthly upriver input, Q_d is discharge from cell exported downriver, Q_g is input from runoff generated within the grid cell, Q_f is exchange between channel and floodplain (plus denotes floodplain to channel), and Q_{dma} is the mean annual downstream discharge. All Q values are in cubic meters per month. The coefficient r_f determines the ratio (0.0 to 1.0) of potential volume change that is assigned to floodplain storage and c_f is the flood initiation parameter, giving the proportion (0.0 to 1.0) of long-term mean annual flow required to invoke floodplain exchanges.

The established topology together with the flow and continuity equations (7a)-(7f) creates a system of linked differential equations. The system is solved for S_c and S_f using a fifth- to sixth-order Runge-Kutta integration technique (International Mathematical and Statistical Libraries, Houston, Texas, 1982). For the entire Amazon / Tocantins basin, 2251 cells are linked. The model applies monthly runoff values for each grid cell until a quasi-steady state solution emerges for the entire set of cells.

The linear transfer coefficient for channel flow, K, can be related to physically meaningful quantities and can assist in subsequent calibration. The continuity equation and the linear model are interrelated as follows:

$$Q_{dma} = V (WH) = 3.86 \times 10^{-7} K (WHLS) \quad (8)$$

where V is mean annual velocity (meters per second), W is channel width (meters), H is water height (meters), L is standard length of grid (meters), and S is a dimensionless expansion factor analogous to sinuosity. The constant is a time scaling factor. Equation (8) reduces to

$$K = 2.59 \times 10^6 (V / LS) \quad (9)$$

Velocity is predicted from Q_{dma} using relationships given by Leopold et al. [1964, footnote to Table 7-21] for a wide spectrum of rivers. An aggregate relation was formulated:

$$\log V = 9.304 \times 10^{-2} \log Q_{dma} - 0.28515 \qquad R^2 = 0.74 \quad (10)$$

Assigning a value of 55 km to L (standard cell length near the equator) permits solution for S as a function of K for particular flows. Figure 4 shows these results. Three flow rates are considered, the mean for all grid cells plus high and low values which bracket the range of possible flow rates. If we interpret the length factor (S) as a measure of sinuosity we can predict a range of candidate K values. It is reasonable to conclude that transfer coefficients lower than about 5/month for low flows and 10-15/month for intermediate and large rivers yield length factors that are inappropriate [Richards, 1982]. We can also define upper limits. K values above 25/month for small rivers, 55 for intermediate rivers and 75 for large rivers yield length factors below 1, a condition that could only exist if the velocity prediction is in some way violated. If we adhere to the velocity predictions, there is then a wide theoretical range for K, on the order of 5-75. Because the model's behavior will be determined most strongly by the mass of intermediate-flow grid cells a reasonable range is likely to be from 15 to 50.

The model was tuned using an unbiased estimator of performance relative to observed data. This index, modified from Willmott [1982] and Willmott et al. [1985b] is

$$d = 1 - \{\sum_1^{12} |P_i - O_i|^y / \sum_1^{12} (|P_i'| + |O_i'|)^y \} \quad (11a)$$

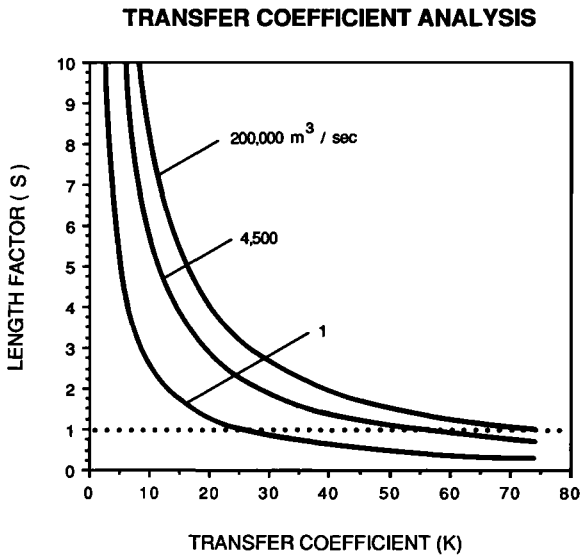

Fig. 4. Relation of fluvial transfer coefficient, K (month^{-1}), to a length scale, S, analogous to sinuosity. Curves bracket the range of flows encountered in this study and define reasonable choices for K in the water transport model. The mean cell discharge is also shown.

$$P_i' = P_i - O_m \quad (11b)$$

$$O_i' = O_i - O_m \quad (11c)$$

where d is the "index of agreement", i is the month, P_i is the i th model prediction, O_i is the corresponding observation, y is an exponent set to 1.0 based on the discussion of Willmott et al. [1985b], and O_m is the observed mean, in this case annual discharge. The d values calculated for each hydrograph were then combined to yield an aggregate measure of model performance. This measure was weighted to combine the effects of flow magnitude and duration of the discharge record. Because of the weighting factors, d values for large rivers and sites with long periods of record were favored.

To produce a best fit, WTM calculations were compared to observed discharge records [UNESCO, 1969, 1971, 1974, 1979, 1985] at six sampling stations. Discharge was expressed as a monthly mean for the period of record. (For Obidos on the mainstem Amazon, the discharge record prior to 1949 was deemed unreliable and therefore deleted from our analysis.) Over 80 model runs were performed with various combinations of the standard channel transfer coefficient and flooding parameters. Minimum to maximum values for the standard K, the flood initiation parameter c_f and the flooding ratio r_f were 12.5 to 50/month, 0.6 - 1.4 and 0.0 - 1.0, respectively. Tests showed that the best model performance (weighted d = 0.136) was afforded by the combination K = 20, c_f = 0.9 and r_f = 0.65.

These parameters defined the standard scenario. A value for K of 20 (residence time of ≈1.5 day for a standard grid) corresponds to the expected values developed earlier. The flooding parameters combine to yield 6-7 months of inundation on the central Amazon. The fitted model indicates how well the combined WBM / WTM structure can reproduce the hydrographic features of the region. Time series data, rather than monthly climatic averages, would be required to test the predictive capacity of the calibration.

The WTM does not currently treat information about hydraulic alteration such as stream diversion or impoundment, although such effects are clearly dominant in other regions. The approach to modeling altered systems would be identical to that developed for unregulated river systems. Namely, an appropriate topology would be developed with mass balance and flow equations. The source / sink terms, however, would need to be modified to accommodate purposeful changes in water use and storage. The inclusion of such information in any continental-scale model represents a formidable data management challenge.

RESULTS AND DISCUSSION

Water Balance Model: General Hydrologic Regimes in South America

The WBM made predictions on approximately 5750 1/2° grid cells in South America. A variety of climatic zones were represented. The bulk of the continent has a single wet ($PPT + R_s \geq PET$) and dry ($PPT + R_s < PET$) season each year. The dominant regime was one in which field capacity was attained during at least one month of the year (11.73 x 10^6 km^2). Areas with snowfall, 0.76 x 10^6 km^2, fell within this category. Field capacity was never attained on 4.14 x 10^6 km^2. A significant subset of cells in this regime had persistent dryness for each month of the year (2.35 x 10^6 km^2). Under such a condition, soil moisture and runoff were set equal to zero and all precipitation inputs, plus any snowmelt, were fully converted into evapotranspiration. Other climatic zones showed more complex behavior with multiple wet and dry seasons each year. Much smaller areas were represented: 0.29 x 10^6 km^2 (FC attained during two wet seasons), 0.40 x 10^6 km^2 (one wet season), and 0.26 x 10^6 km^2 (neither wet season).

For each grid cell, WBM computes the annual mean as well as subannual time series of SM, RO and ET. All such grid-cell-level calculations, when geographically referenced, define the continental-scale hydrology of South America. Figure 5 shows examples of WBM inputs and resulting calculations for grid cells representing the two dominant hydrologic regimes of the continent.

One dominant regime has a single wet / dry season in which field capacity is attained. The representative grid cell is in the Amazon lowland forest (3.0°S, 60.0°W). The predominant soil texture is clay, the rooting depth is 1.2 m and FC is 582 mm of water. This site has a strong signal for seasonal precipitation with relatively uniform PET. The PPT exceeds PET in the single wet season which extends from November through May and is adequate to override any PET deficit incurred during the dry season from June through October. Soil moisture reflects this pattern of water availability. Drawdown begins in June and continues through October to a level 40% below FC. In November and December there is rapid recharge in response to surplus PPT. The maximum,

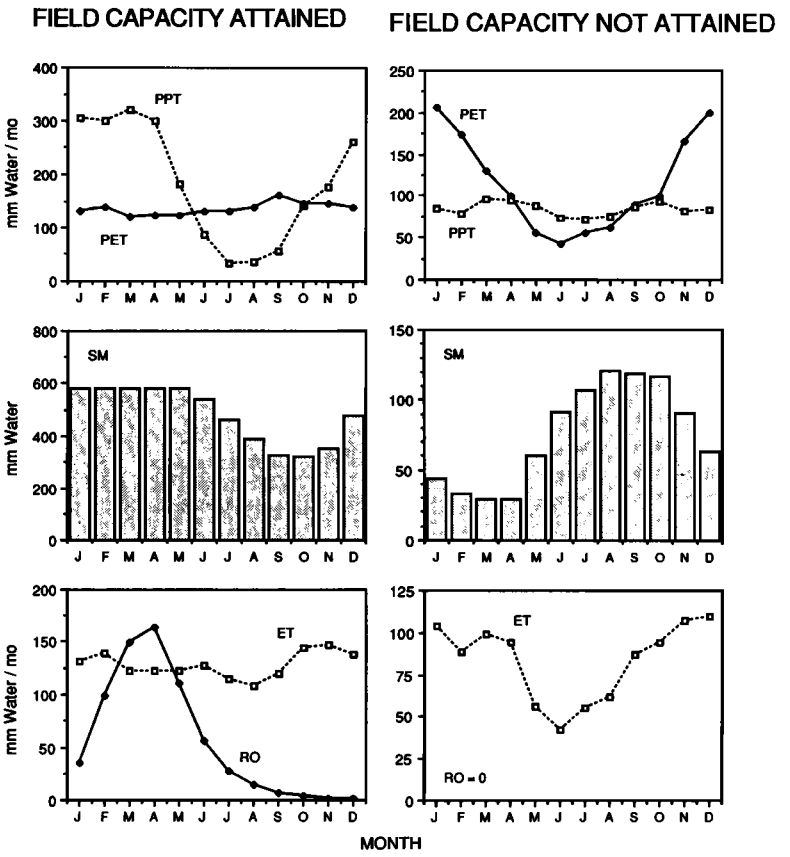

Fig. 5. Water balance model calculations for representative 1/2° grid cells in South America. Each panel displays how the model transforms climatic variables into time series of evapotranspiration (millimeters per month), runoff (millimeters per month) and soil moisture (millimeters). Representative cells are from (Left) the Amazonian rainforest (3.0°S, 60.0°W) and (Right) the Gran Chaco/Pampas region (33.0°S, 58.0°W).

which equals FC, occurs in January and SM remains at this level until the dry season once again begins. During the wet season, ET is equal to PET, and only during the dry season does it fall below the potential. The minimum ET is about 70% of PET. Runoff shows a strong seasonal pattern as well, with values ranging from near 0 to more than 170 mm/month. Although there is ample water surplus starting in January, RO continues to increase due to lags inherent in the linear storage pool. Runoff peaks in April and then decreases in response to smaller excess PPT over PET. Thereafter, RO decays exponentially until January when the soil is once again fully recharged.

A second major regime also has a single wet / dry season but field capacity is never attained. An example of this type of cell is located in the Gran Chaco / Pampas region (33.0°S, 58.0°W). The principal vegetation type is grassland having a 0.7 m rooting depth in a clay soil. The FC is 340 mm of water. This site represents a dry temperate climate in which PPT is relatively low and constant, and PET fluctuates in response to seasonal temperature. Although there is a distinct wet season from May through August total rainfall does not compensate for the effect of PET over the year and SM remains below FC. In fact, moisture stocks in the soil are always far below the 340 mm capacity, with a peak of only 120 mm. From its maximum in August, SM is drawn down to a minimum of 30 mm by April. Evapotranspiration is similarly limited by the lack of available water. The timing of ET follows PET but can only equal the potential during the four-month wet season. Thereafter, ET is limited. In fact, the ET is only 50% of potential in the particularly dry months of January and February. According to the Thornthwaite / Mather model no RO is generated under such dry conditions. Obviously, there is storm runoff in the real world setting and a more complete version of the model would consider such an effect.

Water Balance Model: Detailed Calculations at the Continental Scale

Predictions are presented here for soil moisture, evapotranspiration and runoff in South America. Model results are organized at 1/2° spatial resolution and accommodate the effects of the numerous biogeophysical data sets detailed earlier. Results represent long-term or climatological

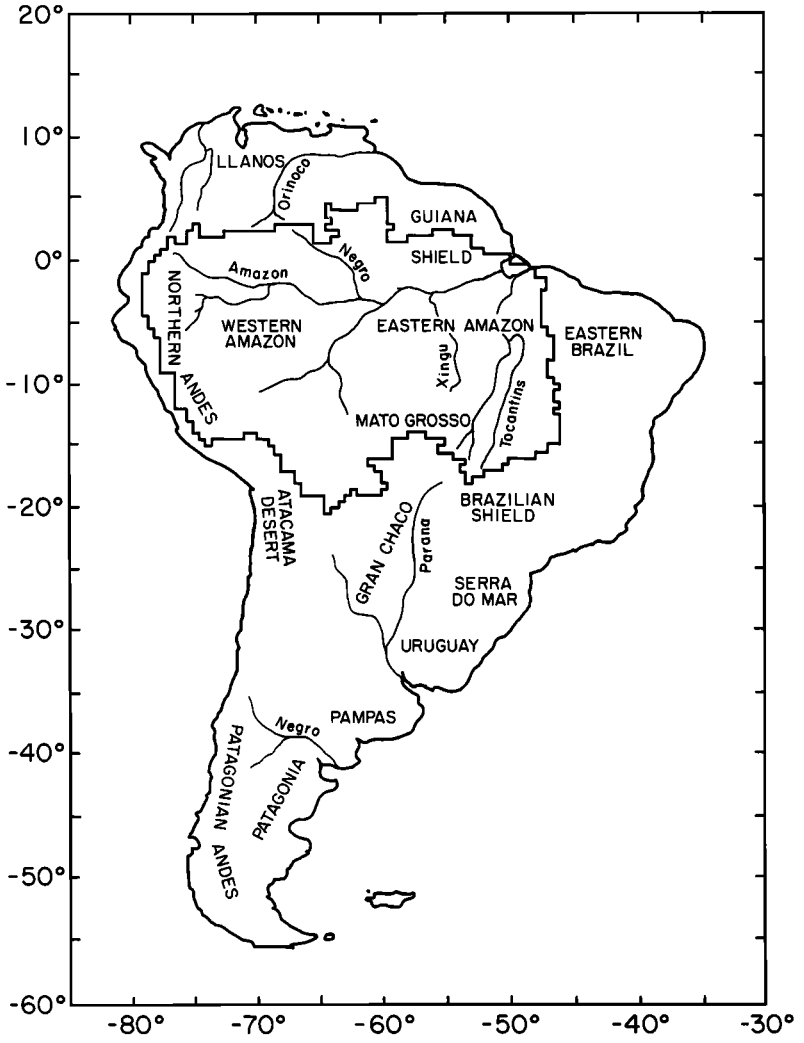

Fig. 6. The major geographic regions of South America.

average conditions. Figure 6 is a map of the broad geographic regions referred to in the discussion that follows.

Soil moisture. Predictions of soil moisture made by WBM are given in Plate 3. Mean soil moisture for the entire continent is calculated as 284 mm, but there are substantial regional differences. The model indicates that mean annual soil moisture is highest in the Western and Eastern Amazon and the southeastern coast of Brazil, and lowest in the Gran Chaco, Pampas and Patagonian regions of Argentina, the Central Andes (with the Atacama Desert) and Eastern Brazil. In addition, the Northern and Patagonian Andes are areas of both high and low SM, owing to steep gradients in climate and soil type. Vast areas have moderate soil moisture. These zones are found over the Mato Grosso, the Brazilian Shield, the northern Guiana Shield and in the northern Llanos.

The WBM map for mean annual soil moisture follows the pattern of precipitation reported elsewhere [Korzoun et al., 1977, Baumgartner and Reichel, 1975]. However, PPT alone is a poor predictor of SM in absolute terms (Figure 7). The PPT dependency becomes more clear if the data are segregated by field capacity (Figure 7). Each graph showing PPT and SM is characterized by three regions. The first is a low variability zone near the origin showing that with little PPT there is little resulting SM. Next is an intermediate zone characterized by higher variability. This zone has the greatest absolute range, suggesting that a variety of other biogeophysical factors are at play in determining mean moisture content. The third zone represents the effect of high precipitation which dampens the variability in SM which is held at or very near field capacity.

Estimates of soil water by WBM were compared to those of Willmott and Rowe [1986] after conversion to 1/2° cells. Willmott and Rowe express soil water from 0 mm above wilting point to 150 mm, an available water capacity applied uniformly to all grid cells. To permit meaningful comparison of the two data sets, we subtracted wilting point values (Table

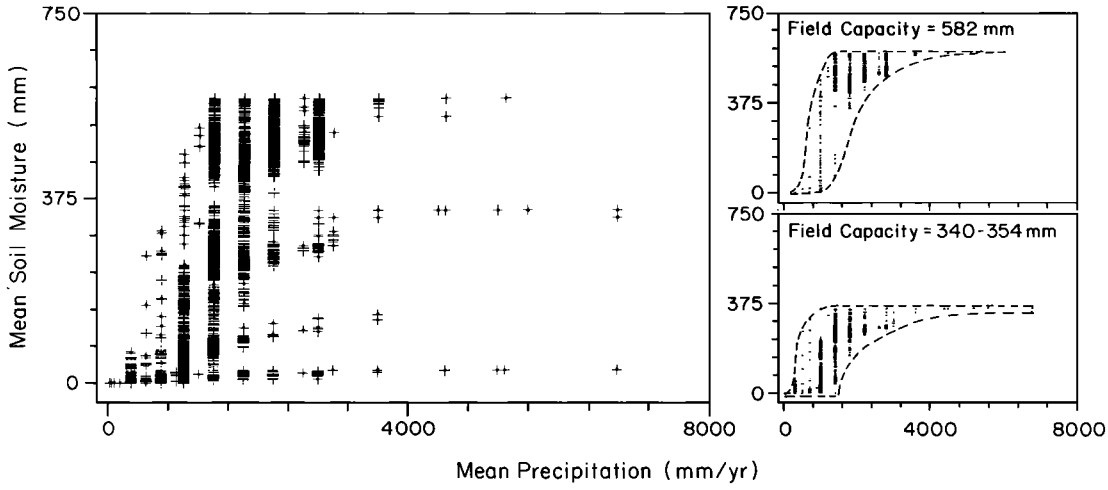

Fig. 7. The relationship between precipitation (millimeters per year) and calculated mean annual soil moisture (millimeters) for grid cells of the South American continent. (Left) All field capacities, (Right) Representative classes.

1) from WBM determinations of SM. The Willmott and Rowe and modified WBM estimates are similar in terms of the spatial distribution of wet and dry soils but their absolute magnitudes often differ substantially. For the entire continent, the two data sets show, respectively, 79 and 35 mm of mean annual soil water. The distribution of numerical differences between the two data sets (Figure 8) is unimodal and reflects the generally lower values determined using WBM. Only 34% of WBM grid cells have soil water values greater than those of Willmott and Rowe. These cells are evident where Willmott and Rowe predict relatively high soil water (≥ 75 mm), generally forested areas with high rainfall and, in the case of WBM, available water capacities in excess of 150 millimeters (Table 1). The majority of WBM predictions are lower than those of Willmott and Rowe in drier areas (< 75 mm soil water). This reflects not only differences in PPT and PET data fields but also the ability of the Thornthwaite and Mather model to draw soil moisture stocks below wilting point.

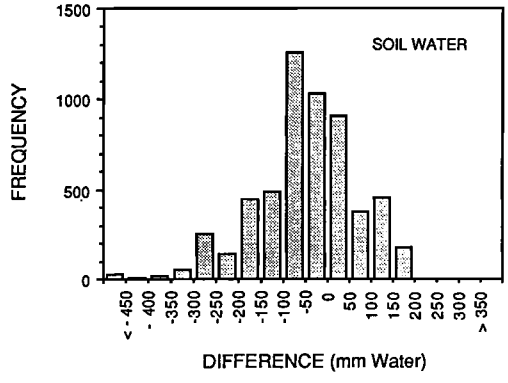

Fig. 8. Correspondence between soil moisture estimates made by the water balance model and Willmott and Rowe [1986]. Each difference value (millimeters) is computed as WBM value minus Willmott and Rowe value.

The seasonal pattern of soil moisture is summarized using four representative months (Plate 3). For much of the continent, moisture values are surprisingly stable. This constancy is associated with broad regions of moderate to high mean annual SM, namely, the Western Amazon basin, much of the southeastern Brazilian Shield and portions of the Northern and Patagonian Andes. Over much of this area, soils are at or near field capacity throughout the year. Relatively dry and stable areas are the Gran Chaco Plains, the Pampas and the central Andes. Areas within the Northern Andes have persistently low SM because of the limited 27 mm field capacity of lithosols.

More dynamic soil conditions dominate much of Eastern Brazil, the Guiana Shield, the Eastern Amazon and the Mato Grosso. For most of these regions April is the wettest month and relatively dry areas are found only in extreme Eastern Brazil, the fringe of the Gran Chaco and the northern Guiana Shield. By July, the area of drying soils expands and major portions of the Amazon, Brazilian Shield and Mato Grosso show net depletion. Predictions for October indicate an expansion and intensification of the drying zone that influences most of these regions. By January each region has a net increase in soil water and the extent of dry zones diminishes dramatically. In contrast, the timing of such changes in soil moisture is offset by approximately three months for the Guiana Shield, due to changes in the position of the intertropical convergence zone. In areas where the variations in calculated SM are substantial the seasonal pattern is correlated with the seasonality of precipitation [Korzoun et al., 1977].

Evapotranspiration. WBM determinations of mean annual ET and its fluctuation over the year are shown in Plate 4. The broad pattern of ET is influenced by the distribution and timing of precipitation, potential ET and buffering capacity of the soil moisture pool. On a continental scale, mean ET was predicted by WBM to be 1059 mm/yr or approximately 80% of potential ET.

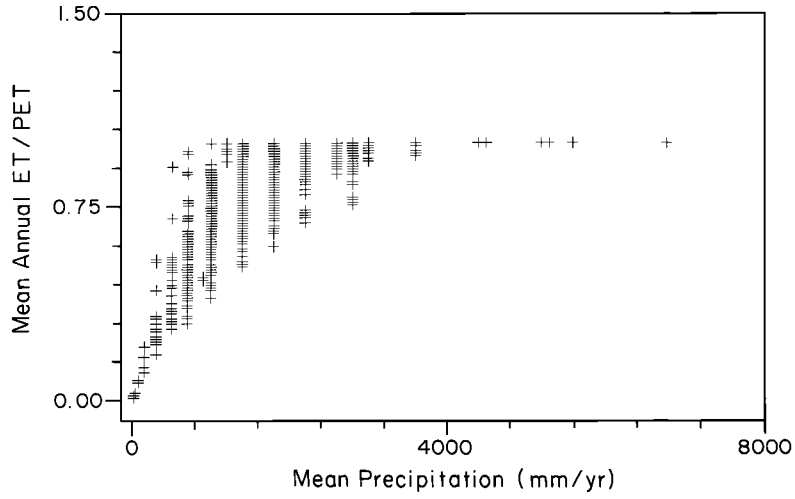

Fig. 9. The relationship between precipitation and computed evapotranspiration for grid cells of the South American continent. The abscissa is precipitation; the ordinate is the fraction of potential ET that is computed to actually be lost from the soil as evapotranspiration. Potential ET, actual ET and precipitation are in millimeters per year.

Because of surplus PPT, large sections of the continent have predicted ET values only modestly reduced from PET. The best example of this is the Western Amazon where ample rainfall fully satisfies (within the bounds of map resolution) the PET demand. Other areas where this is true are the Northern Andes, portions of the Patagonian Andes, the Guiana Shield, the Llanos region of Venezuela and the coastal region from Eastern Brazil to Uruguay. The southernmost tip of the continent has a wet climate and almost completely satisfies the modest potential ET demands driven by a cold climate.

Mean annual ET is substantially reduced from PET in areas where PPT is limited and the dry season(s) dominates. Predictions for Eastern Brazil, the Pampas, and the Atacama Desert therefore all show this effect. The Guiana Shield, the Mato Grosso and the Brazilian Shield are locations of more moderate rainfall (relative to PET) and therefore the PET is altered less drastically. In these areas, ET is neither unlimited by ample rainfall nor severely constrained by its scarcity.

The calculated geographical distribution of mean annual ET suggests that it is strongly related to PPT. Figure 9 shows the predicted fraction of PET that emerges as ET expressed as a function of PPT for all South American grid cells. The plot provides a check on the ability of WBM to calculate reasonable ET estimates over a broad range of climatology. As expected, ET is strongly controlled by PPT in both very dry and very wet grid cells. The high variance in ET / PET for cells with intermediate PPT is due to the influence of wet and dry season timing and soil water retention.

WBM predictions of ET can be compared to the Korzoun et al. [1977] and Willmott and Rowe [1986] data sets. Overall, the three data sets are comparable in magnitude (computed ET ranged from 880 to 1060 mm/yr) and the spatial distributions match best in areas of low ET. The spatial patterns match more poorly in regions of moderate to high ET. Although the spatial distributions of ET are most similar between WBM and Korzoun et al., ET for South America is predicted to be higher with WBM (Figure 10). The mean ET for the entire continent given by Korzoun et al. is 882 mm/yr, compared to 1059 mm/yr for WBM. The bulk of the differences between the two data sets ranges from -200 to +600 mm/yr (WBM values minus Korzoun et al. values). The differences show no systematic pattern in relation to the magnitude of ET. A comparison of WBM calculations to those made by Willmott and Rowe yields a different picture (Figure 10). The disparity is now nearly unimodal, with WBM showing systematically higher estimates of ET. The mean ET predicted by Willmott and Rowe is 997 mm/yr, falling between WBM and Korzoun et al. predictions. The range of disparity is greater than in the previous comparison, mainly from -600 to +600 mm/yr (WBM values minus Willmott and Rowe values) although the mean difference is only +62 mm/yr. As in the previous comparison, differences in the WBM / Willmott and Rowe contrast were not clearly related to the magnitude of ET.

The disparities among the three data sets are difficult to trace and are a complex function of the manner in which soils and climatology interact in each study, and any interpolation of ground-based data. Nonetheless, WBM compares favorably with these established data sets. On a continental basis, WBM estimates for mean annual ET fall within 20% and 6% of estimates of Korzoun et al. and Willmott and Rowe, respectively.

The temporal distribution of ET over the continent was also analyzed (Plate 4). There are two major contiguous zones with nearly constant ET: the northernmost Andes / Western Amazon / Orinoco region for high ET and Patagonia / Pampas / Atacama Desert region for low ET. These extremes reflect the availability of PPT in these areas. In persistently wet zones PET is nearly unlimited and ET is high; in very dry areas soil water retention limits ET. The remainder of South America displays distinct seasonal patterns. Examples are the Eastern Amazon, the Guiana Shield, Eastern Brazil, the Brazilian Shield and the Gran Chaco. These are areas in which there is a strong seasonality of PPT. With the excep-

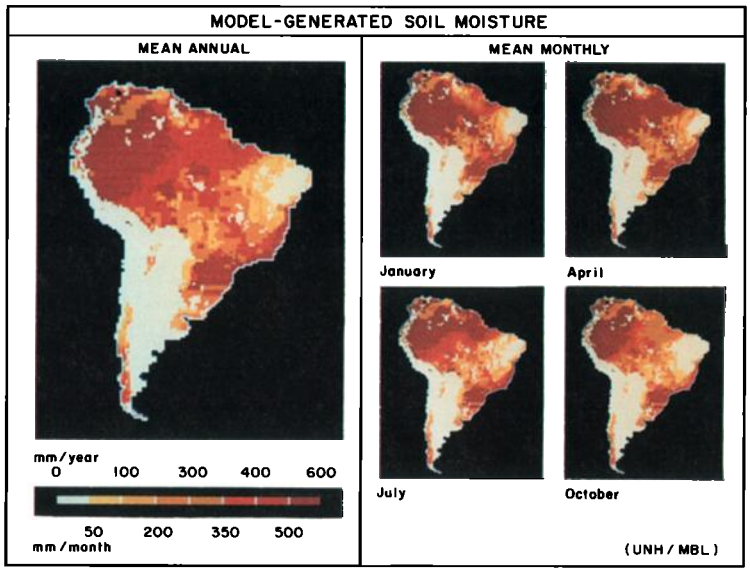

Plate 3. Mean annual and monthly soil moisture predicted by the water balance model at 1/2° spatial resolution. Maximum values correspond to field capacities shown in Plate 1. Predictions are independent of floodplain inundation.

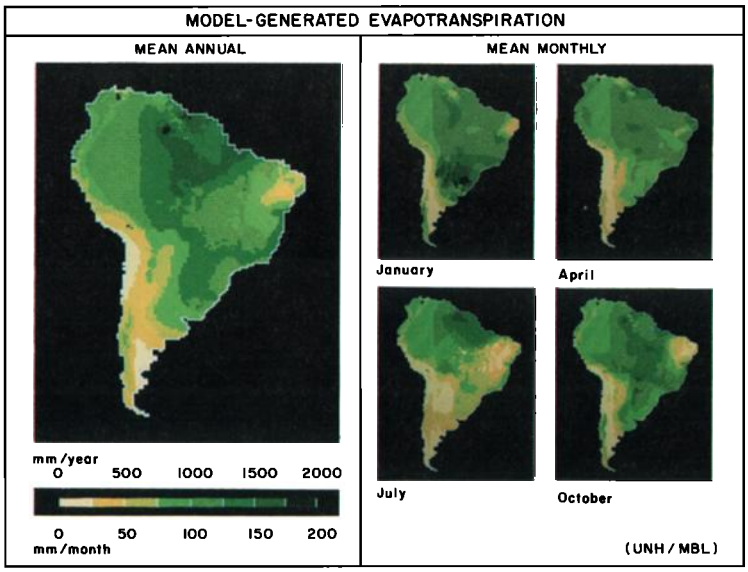

Plate 4. Mean annual and monthly evapotranspiration predicted by the water balance model at 1/2° resolution.

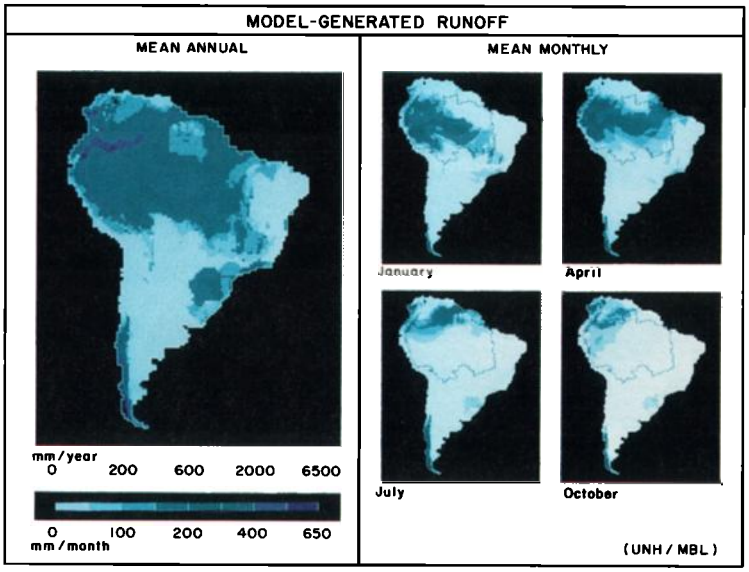

Plate 5. Mean annual and monthly runoff predicted by the water balance model at 1/2° resolution. The Amazon / Tocantins drainage basin is outlined

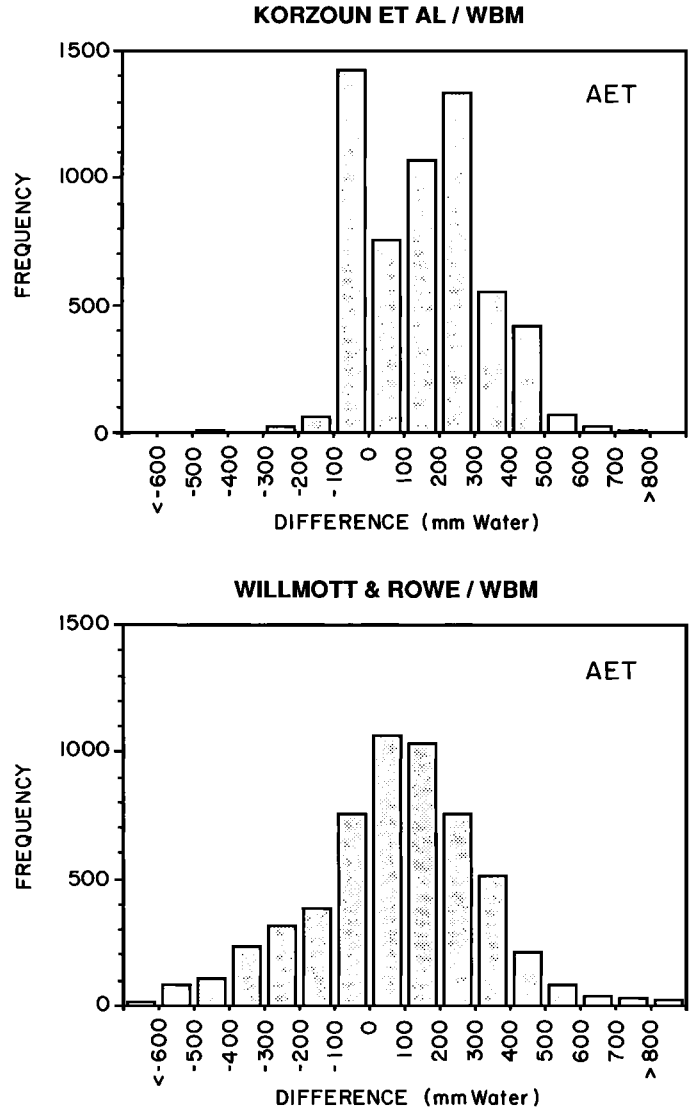

Fig. 10. Correspondence between evapotranspiration determined by the water balance model, (Top) Korzoun et al. [1977] and (Bottom) Willmott and Rowe [1986]. Each difference value (millimeters per year) is computed as WBM value minus Willmott and Rowe value and as WBM value minus Korzoun et al.value.

tion of Eastern Brazil and the Gran Chaco (which show peak ET in summer and fall), the more seasonal areas display highest ET in the winter and spring.

Runoff. Continental runoff for South America (Plate 5) was computed to be 619 mm/yr, representing 37% of total precipitation. Mean annual RO is spatially correlated to continental PPT. Thus, areas within the Amazon and Orinoco catchments, the Serra do Mar, and the Northern and Patagonian Andes, show high annual RO. The regions contributing least RO encompass Eastern Brazil, the Pampas and Gran Chaco Plain in Argentina, and the Atacama Desert. Large areas of the continent (5.65 x 10^6 km^2) show less than 100 mm/yr RO. Intermediate values are apparent in the Guiana and Brazilian Shields, the Mato Grosso and the northern Llanos, regions which have a relative balance between PPT and PET. These areas correspond to those with intermediate SM shown in Plate 3.

A strong relationship exists between PPT and computed mean annual RO for South American grid cells (Figure 11). The distribution of points begins near the origin, passes through a zone of increased variability and finally ends as a nearly straight line with slope close to 1. At low values of PPT, little RO is generated since most PPT is conveyed to soil moisture recharge and ET. At intermediate levels, there is a more variable response associated with more variable ET and SM dynamics, which in turn determine the availability of

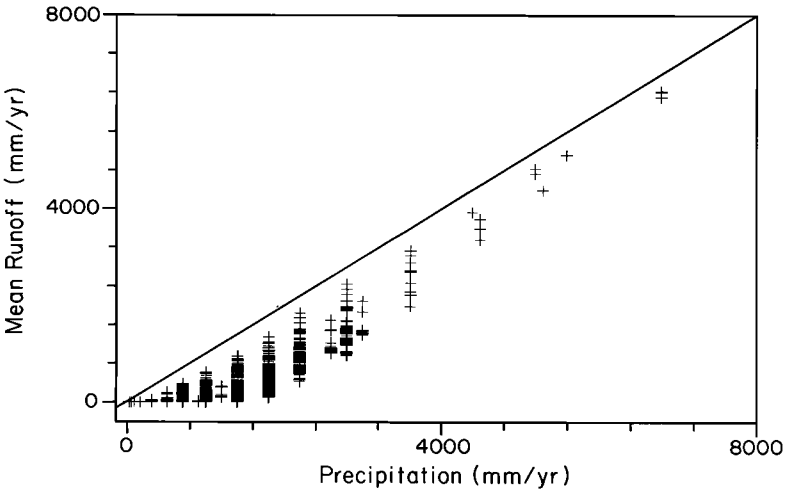

Fig. 11. The relationship between precipitation and model-derived runoff for grid cells of the South American continent. All values are in millimeters per year.

surplus water. At the highest PPT values, soil moisture approaches field capacity and increases in PPT result in linear increases in RO since ET and soil storage are near their maximum. This same finding is reported for South America using a climate model [Dickinson and Henderson-Sellers, 1988] and has been observed at a more local scale [FAO / United Nations Development Program (UNDP), 1968; Likens et al., 1977; Havel and Bligh, 1982].

We compared runoff generated by WBM to an observational data set from Korzoun et al. [1977], based on contoured data from 236 hydrographic monitoring stations having a range of 4 to 63 years of record. The correspondence is extremely close, both in terms of spatial pattern and magnitude. For the continent as a whole, WBM runoff is slightly lower than that of Korzoun et al. Areas of high RO correlate best; namely the Amazon basin, the Patagonian and Northern Andes and the Serra do Mar. WBM predicts a slightly larger area with sparse RO for the Gran Chaco, Pampas, portions of the Northern Andes, Patagonia and Eastern Brazil. Regions of intermediate RO, such as those within and immediately surrounding the Brazilian and Guiana Shields, show significantly greater spatial detail with WBM.

The data in Figure 12 further demonstrate a close correspondence between the two data sets. The frequency plot shows that the disparities (WBM values minus Korzoun et al. values) have a unimodal distribution centered about the 0 to -200 mm/yr class with the bulk of the differences lying within +/- 600 mm/yr. For the continent as a whole, the mean disparity is -73 mm/yr or 11% of the observed continental runoff (692 mm/yr). In grid cells reported by Korzoun et al. to have ≤1000 mm/yr RO, WBM calculates slightly lower RO values relative to the observational data. The effect can be

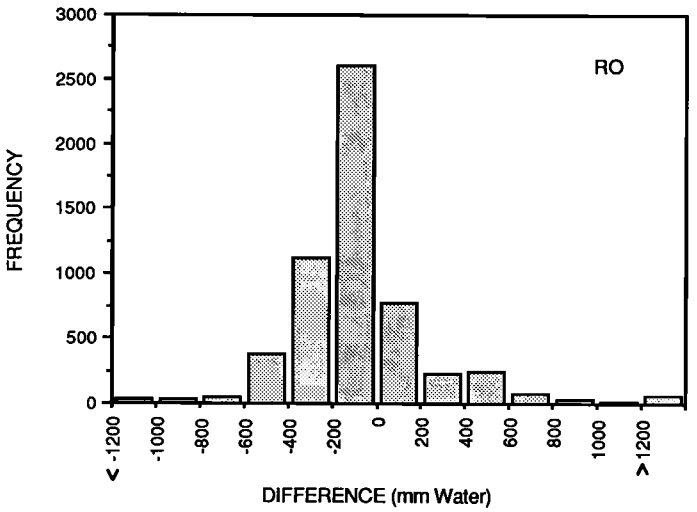

Fig. 12. Correspondence between runoff estimates made by the water balance model and Korzoun et al. [1977]. Each difference value (millimeters per year) is computed as WBM value minus Korzoun et al. value.

traced to assumptions regarding the absence of storm flow in WBM for drier regions. In wetter areas (> 1000 mm/yr RO), differences between the two data sets are centered more closely about zero.

The seasonal pattern of RO was calculated by WBM (Plate 5). A striking feature of the maps is the relative constancy of RO for major portions of the continent over the year. These areas are dry and include Eastern Brazil, the Gran Chaco, the central Andes, Pampas and Patagonia. Another area of relative stability is the wet Patagonian Andes which shows only slight seasonality, being driest in the early part of the year and wettest in July due to low PET demands associated with the southern hemisphere winter. Seasonal RO dynamics are most complex in the equatorial zone, from about 10°N to 20°S. Only in the northernmost Llanos region does RO appear relatively constant.

Water Balance Model: Amazon / Tocantins Drainage Basin

The dominant runoff-producing region is the Amazon / Tocantins drainage system. The combined basin had a mean annual RO of 1.01 m, with 1.08 m in the Amazon basin, and 0.56 m in the Tocantins. The value of 1.01 m/yr compares favorably with other hydrologic studies as reported by Salati [1985]. Runoff values for the entire basin, based on a variety of methods, fall within the range of 0.7 to 1.25 m/yr. WBM-generated runoff, expressed as an annual mean for the combined basin, corresponds to a net discharge to the ocean of 224,000 m^3/s. The Amazon itself contributes 207,000 m^3/s and the Tocantins 17,000 m^3/s.

Precipitation entering the Amazon / Tocantins region delivers 2.26 m of water on an annual basis. Predicted ET accounts for 1.24 m. Fifty-five percent of the precipitation delivered to the simulated Amazon / Tocantins Basin thus emerges as ET and 45% as RO. These percentages are nearly identical for the basins considered separately. WBM predictions agree with other regional analyses. For example, Salati [1985] cites a series of estimates showing ET / RO ratios from roughly 50/50 to 70/30. Salati's basinwide estimate is 54/46, nearly identical to that found in this study.

The temporal pattern of RO reflects a shifting mosaic of source areas that is important in defining the pattern of fluvial transport. Throughout much of the region, the early part of the year shows significant RO (> 50 mm/month). January and April are the wettest months and a decided movement northward in runoff-producing regions is apparent. By July, the runoff-generating zone moves northward and only the most northern areas of the basin contribute any significant RO. By October, the majority of the basin is relatively dry and fails to generate significant runoff. Only the far western area is active. These patterns agree well with observed patterns of monthly RO given elsewhere [Korzoun et al., 1977; UNESCO, 1969, 1971, 1974, 1979, 1985]. The WBM determinations also correlate well with the climatology of the region [Salati and Marques, 1984; Salati, 1985].

Water Transport Model: Amazon / Tocantins River

The WTM computed discharge hydrographs for each of the 2251 grid cells of the Amazon / Tocantins river system. Results are summarized in this section using site-specific data. We first compare model performance to a set of observed hydrographs, go on to discuss the seasonality of discharge in major tributaries and the mainstem, and finally perform a sensitivity analysis to explore the nature of computed channel flow and the importance of floodplain inundation.

Comparison to observed hydrographs. Because there are few reliable discharge estimates for the Amazon / Tocantins River system it is difficult to assess fully the accuracy of the WTM. Model results were compared initially to ten discharge hydrographs compiled from UNESCO [1969, 1971, 1974, 1979, 1985] using the parameterization described earlier. Four of the sites were located in the Andes where sharp climatic gradients and complex drainage patterns restricted the effectiveness of the transport model. Two of the Andean sites were associated with rivers that drained catchments much smaller than the size of a single 1/2° grid cell. The transport model thus performed poorly in these areas (average unweighted d = 0.57; equation (11)). In contrast, the remaining six sites represent larger basins with more clearly defined routing and, generally, longer periods of record. These showed improved model performance (d = 0.76).

On a mean annual basis, calculated discharges for the Obidos, Araguaia, Porto Nacional, Itupiranga, Xingu and Madeira sites were, respectively, within 1, 3, 6, 18, 28 and 33% of the corresponding observed discharges (Figure 13). Predictions for the timing of subannual discharge corresponded well with observation for all sites. However, slight disparities in this timing and in the overall magnitude of discharge, can result in relatively large errors in absolute terms. The above sites, respectively, showed mean average error (MAE) values of 13550, 1120, 1110, 5370, 4040 and 5620 m^3/s. (Mean average error is defined as

$$MAE = N^{-1} \sum_{1}^{N} | P_i - O_i | \qquad (12)$$

from Willmott [1982]. N is the number of observations, P_i is model prediction for month i, O_i is corresponding observed discharge.) For all sites, there is a tendency for the WTM to underestimate during periods of low flow, an effect linked in part to the WBM protocol restricting storm flow during the dry season. The quality of simulated discharges made for the period of higher flow is more variable.

Overall, the Obidos site performs best, with both the timing and magnitude of flow closely following the observed hydrograph. The hydrograph generated for the Araguaia site also matches observation, although a slight lag in peak flow is apparent. The timing of calculated flows at the Madeira site corresponds well to observation although the overall magnitude of the modeled discharge is low. The shape of WTM hydrographs for the remaining sites — Xingu, Itupiranga and Porto Nacional — are less precise, but considering the short period of record (1976-1979), comparisons may be misleading. The largest disparity between WTM and observed discharges is associated with peak flow. For Porto Nacional, this merely represents a timing issue. In the case of Xingu and Itupiranga, the disparity also reflects overestimates in calculated annual discharge.

Such "errors" can be corrected by judicious choice of parameters in the water balance model, the transport model or

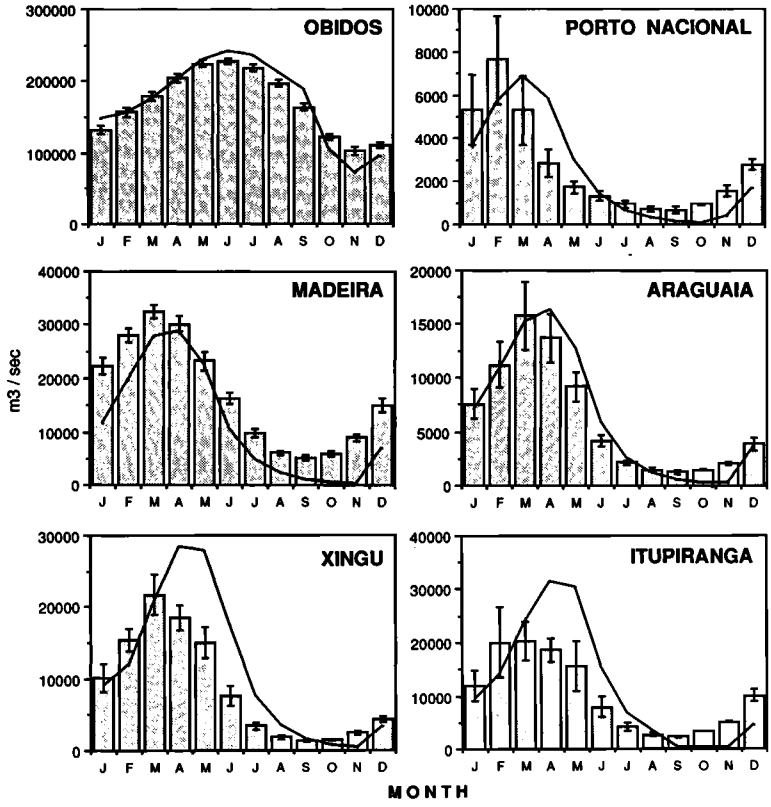

Fig. 13. Modeled and observed discharge hydrographs for selected sites in the Amazon and Tocantins River system. Model predictions (lines) represent the best aggregate fit of the fluvial transfer and flooding coefficients. Observed data (bars) are from UNESCO [1969, 1971, 1974, 1979, 1985] for the following periods of record: Obidos (1969, 1971-1978), Madeira (1968-1979), Xingu (1977-1979), Porto Nacional (1976-1979), Araguaia (1976-1979), Itupiranga (1976-1979). The first three sites are in the Amazon Basin; the latter three are in the Tocantins.

both. Lacking a comprehensive basin-wide data base, no recalibration was attempted. Further, the modeling analysis is based on long-term climatic conditions with natural vegetation; observed hydrographs are influenced by ongoing changes in land use [Gentry and Lopez-Parodi, 1980]. The results presented therefore represent the inherent resolution of our coupled WBM / WTM algorithm and limitations in the associated data sets. Nonetheless, WBM / WTM provides an excellent prediction of observed monthly discharges at major sampling stations in the Amazon / Tocantins River system. For the six hydrographs we found a highly significant relationship, with slope ≈ 1, between observed and calculated monthly discharge: *obs* (m^3/s) = 0.957 *calc* - 1519.8 (R^2 = 0.99 ; n = 72 ; $p << 0.001$).

Qualitative comparisons were made using normalized hydrographs and corresponding observations found in the work by Korzoun et al. [1977] (Figure 14). There was considerable difficulty in determining the specific location of the observed time series, and there was no information on the period of record nor on the magnitude of flow. As best we could determine, the sites are associated with relatively small catchments with 30 to 600 m^3/s mean annual flow. Despite these limitations on the comparison, there is good agreement between model results and observed patterns of discharge.

Model-generated discharge hydrographs at eleven mainstem Amazon and two Tocantins locations are presented, along with estimated discharges for the mouth of each system (Table 3). Upriver sites represent the locations of major confluences and include flows derived from the named tributaries. When corrected for tributary effects, the calculated mainstem hydrographs for Ica, Negro, and Obidos correspond closely to hydrographs presented by Richey et al. [1986] for 1982-1984.

Model estimates for monthly and mean annual flow on thirteen major tributaries of the Amazon River are summarized in Table 4. For each tributary strong seasonal patterns are apparent, related to both the mosaic of WBM-generated RO and transport of this RO within the river network. For both northern and southern tributaries there is a west to east movement in the timing of peak and low flows which correspond to inputs from WBM. The northern tributaries show this effect most clearly with a 2-3 month lag from western to eastern sites. The southern tributaries act more in unison, with peak and low flows displaced by only 1-2 months.

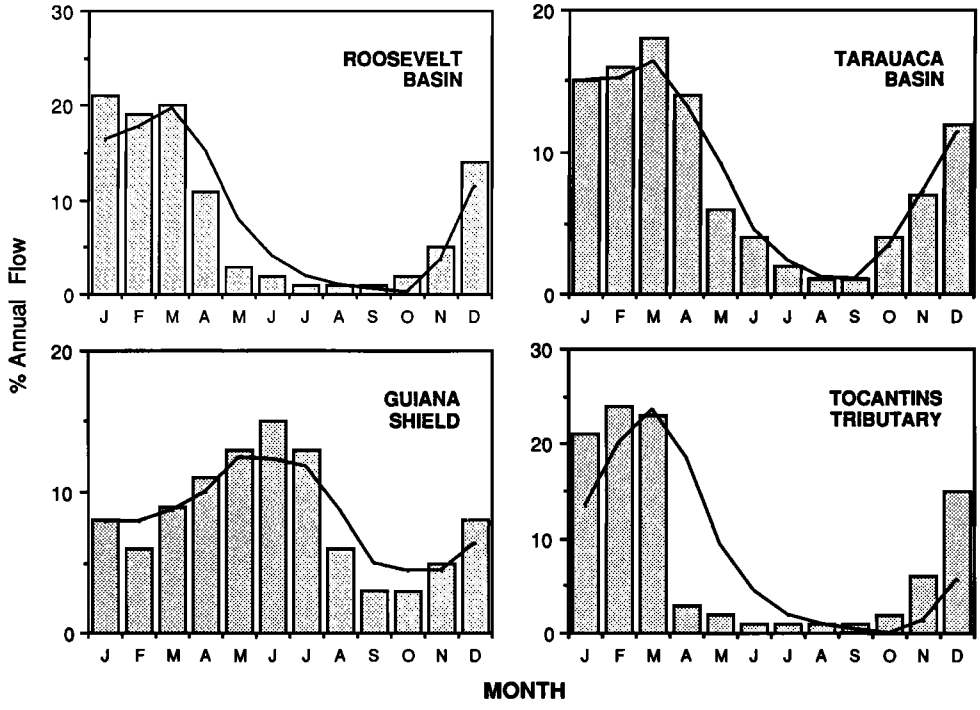

Fig. 14. Normalized discharge hydrographs comparing WTM calculations (lines) to observations (bars) at selected sites within the Amazon and Tocantins drainage basins. Model estimates represent the best aggregate fit of the fluvial transfer and flooding coefficients. Observed data are from Korzoun et al. [1977]. Except for the Tocantins tributary, all hydrographs are in the Amazon Basin proper.

The tributary dynamics suggest that a flood wave will appear in the western portion of the mainstem and progress eastward over the year. The model simulates this effect (Table 3) and shows that there is a distinct lag between peak flows as the flood wave travels eastward from May (Napo, Javari) to July (mouth). Low flows originate in September in the west, and the basin mouth shows minimum discharge in December.

Mainstem / tributary interactions. We can explore in more detail the impact of modeled tributary inputs on the behavior of the mainstem Amazon, and estimate the degree to which the main river can buffer tributary inputs. Table 5 shows a longitudinal profile of discharge variability at a series of mainstem sites and contrasts this with influent variability. The months of maximum flow and the proportion of mainstem flow attributed to each tributary are also shown.

There is a general tendency for the Amazon River to decrease its subannual variability (measured by V^m) from the westernmost site to the Madeira confluence, where there is a sharp reversal in the dampening trend. The tributaries show no clear longitudinal pattern of variability over the same region. In all but one case, the mainstem has greater variability than its tributaries, from both the north and south. Downstream of the Madeira to its mouth, the Amazon maintains a consistent degree of seasonal oscillation and there is no apparent dampening of the flood wave. However, the mainstem is consistently less variable than its tributaries and dampens well the input signals.

Calculated tributary inputs are important in determining the timing of the peak flows on the mainstem Amazon. From the Napo to Japura sites there is an orderly progression downstream of the peak flood wave in May and June and the timing coincides with that of tributary inputs which are sizable fractions of the overall mainstem flow. From the Purus to Madeira sites, flood wave timing is more variable and is shifted either forward or backward in time depending on the behavior of the tributary inputs. For example, at the Purus site the mainstem peaks in May, one month earlier than at the adjacent upriver site, in apparent response to an early peak in tributary discharge during April. Downriver of the Madeira, tributary inputs are relatively small and the mainstem flood wave propagates independently. The time of highest discharge shifts forward from May to July in the mainstem reach from the Madeira to the mouth.

The mainstem Amazon is therefore most influenced by the behavior of its tributaries in the western portion of the basin. The tributaries control the timing of the mainstem flood wave and the mainstem does not appear to dampen its tributary signals in its upstream reaches. In contrast, the river downstream of the Madeira confluence is stable, dampens variability in its tributary inflows and is unaffected by the timing of these inputs.

Sensitivity to transfer and flooding parameters. We examined the sensitivity of the fluvial model to variations in the linear transfer coefficient (K) and the parameters defining floodplain inundation (c_f, r_f) given in (7). The analysis

TABLE 3. Model-Generated Discharges for the Mainstem Amazon and Tocantins

Confluence Site Name	Grid Cell[a] (Latitude/Longitude)	Flow Rate, (10^3 m^3/sec) Jan.	Feb.	March	April	May	June	July	Aug.	Sept.	Oct.	Nov.	Dec.	Annual Mean
						Amazon River								
Napo	3.5°S/73.0°W	40.3	46.8	57.4	67.5	69.1	48.3	26.7	13.5	10.5	17.1	31.1	36.4	38.7
Javari	4.5°S/70.0°W	46.1	49.8	57.6	68.2	76.7	73.8	46.0	23.9	16.0	18.0	32.5	42.3	45.9
Ica	3.5°S/68.0°W	57.7	62.2	66.8	76.0	86.6	90.9	77.3	41.6	24.8	23.4	38.4	52.3	58.2
Japura	3.5°S/65.0°W	85.0	95.8	104.7	111.0	120.1	127.4	122.3	88.6	47.0	35.5	53.3	78.3	89.1
Purus	4.0°S/61.5°W	101.0	112.3	128.4	141.5	145.7	143.6	137.3	127.7	72.9	44.1	49.4	87.5	107.6
Negro	3.5°S/60.0°W	123.1	133.4	149.7	166.7	175.1	178.5	175.8	172.5	123.9	74.0	66.4	103.7	136.9
Madeira	3.5°S/59.0°W	150.9	167.5	193.0	220.4	234.4	230.6	208.7	187.9	142.2	80.3	68.5	116.4	166.7
Trombetas (Obidos)	2.0°S/56.0°W	148.2	155.9	174.9	203.1	230.0	241.2	235.7	213.0	189.6	105.0	71.7	96.4	172.1
Tapajos	2.5°S/55.0°W	159.4	173.0	195.3	230.5	261.0	271.1	253.3	227.5	199.2	116.6	76.5	99.6	188.6
Xingu	2.0°S/52.5°W	154.7	180.5	198.4	237.8	278.7	298.6	283.9	255.9	224.0	151.1	86.5	87.0	203.1
Mouth	0.5°N/50.0°W	126.1	177.1	186.3	201.3	236.6	275.6	296.9	288.5	262.5	227.0	118.8	82.4	206.6
						Tocantins								
Araguaia/ Itacaiuna	5.5°S/49.5°W	9.3	14.2	23.9	31.4	30.4	15.4	6.8	3.4	0.4	0.3	0.3	4.4	11.7
Mouth	0.5°S/48.5°W	7.3	14.2	18.2	28.7	38.7	40.5	32.6	14.5	6.1	2.5	1.0	1.0	17.1

Discharges are calculated below the confluence of the named tributary.
[a]Latitude/longitude values refer to southwest corner of grid cell.

TABLE 4. Model-Generated Discharges for Major Amazon River Tributaries

Name	Grid Cell[a] (Latitude, °S/ Longitude, °W)	Flow Rate, 10^3 m^3/s Jan.	Feb.	March	April	May	June	July	Aug.	Sept.	Oct.	Nov.	Dec.	Annual Mean
						Northern Tributaries								
Napo	3.5/73.5	8.1	7.7	9.1	10.2	10.8	10.2	7.7	4.3	3.2	4.0	7.1	7.9	7.5
Ica	3.0/68.5	10.2	10.4	10.0	10.3	11.0	11.1	10.5	7.4	4.9	5.1	7.7	8.6	8.9
Japura	2.0/66.5	16.8	17.8	16.7	16.8	19.0	20.4	17.3	11.2	7.3	9.1	12.5	13.9	15.0
Negro	3.0/61.0	23.8	26.0	27.9	28.9	29.9	32.8	36.5	39.5	28.2	24.2	20.4	22.2	28.4
Trombetas	1.5/56.5	0.1	0.0	0.1	1.2	2.6	3.2	3.5	2.6	1.3	0.6	0.3	0.1	1.3
						Southern Tributaries								
Marañon	5.0/74.5	18.8	23.1	28.5	32.3	28.9	16.4	8.8	4.4	3.9	7.2	12.6	15.6	16.7
Ucayali	5.5/74.5	15.2	19.1	23.6	25.4	21.1	9.8	4.5	2.1	2.3	5.2	10.8	12.6	12.6
Javari	4.5/71.0	5.1	4.8	5.5	5.5	4.7	2.5	1.6	1.2	1.8	2.5	3.7	4.7	3.6
Jurua	3.0/66.0	11.2	14.2	17.2	18.7	18.3	12.8	5.8	2.7	1.6	2.8	6.6	9.3	10.1
Purus	4.5/62.0	15.9	20.6	25.9	29.3	27.5	18.4	8.1	3.6	1.6	0.8	3.5	12.7	14.0
Madeira	4.0/59.5	26.7	35.2	44.7	54.2	56.6	47.4	24.4	10.5	4.5	1.9	3.3	16.2	27.1
Tapajós	3.0/55.5	14.6	19.9	27.6	34.9	36.0	28.3	12.3	5.4	2.4	1.3	2.3	9.7	16.2
Xingu	2.5/52.5	8.4	11.1	18.6	28.4	31.6	24.1	10.6	4.6	2.0	0.9	0.5	2.6	12.0

Discharges are calculated at the mouth of each tributary and prior to entering the mainstem.
[a]Latitude/longitude values refer to southwest corner of grid cell.

TABLE 5. Influence of Tributary Inputs on the Behavior of the Mainstem Amazon River

Site Name[a]	V^M	V^T	Flow Proportion[b], %
Napo	1.51 (May)	1.01 (May)	19
Javari	1.32 (May)	1.19 (April)	8
Ica	1.16 (June)	0.70 (June)	15
Japura	1.03 (June)	0.87 (June)	17
Purus	0.94 (May)	2.04 (April)	13
Negro	0.82 (June)	0.67 (Aug.)	21
Madeira	1.00 (May)	2.01 (May)	16
Trombetas (Obidos)	0.98 (June)	2.69 (July)	1
Tapajos	1.03 (June)	2.14 (May)	9
Xingu	1.04 (June)	2.59 (May)	6
Mouth	1.04 (July)	---	---

V^M is the variation in mainstem discharge over the year ($V^M = (Q_{max}-Q_{min})/\bar{Q}$) at each site. V^T is same as V^M but for tributary.

[a]Refers to confluence site on mainstem for V^M; to mouth of tributary for V^T.

[b]Calculated as Q_{trib}/Q_{main}, where mainstem flow includes Q_{trib}.

[c]Month of peak discharge.

sought to identify reasonable rates of water turnover and the importance of wetland flooding in the Amazon River system.

For experiments involving the transfer coefficient we examined the resulting flow at Obidos when K was varied from 12.5 to 75/month, with c_f set to 1.0 and r_f to 0.75 (Figure 15). The effect of the transfer coefficient is to regulate both the timing and amplitude of the discharge wave. Starting with K = 75 there is a significant overestimate of high flow, an early maximum in April and a minimum in September. With decreasing K values (from 37.5 to 25) the peak diminishes and is offset forward in time. Low flows are preserved but occur later in the year. For K = 12.5, the shape of the hydrograph is clearly inappropriate. A range of $12.5 < K < 75$ appears to offer reasonable results and is in agreement with the theoretical range developed earlier.

Experiments testing the importance of wetland flooding are also shown in Figure 15. The first scenarios involve c_f, which initiates floodplain inundation. The graph shows the effect of limiting the flood cycle. The case of no flooding gives a smooth nearly sinusoidal curve with a range from 50,000 to 300,000 m^3/s. By selectively varying the proportion of mean annual flow at which flooding can occur, the hydrograph can be dampened and altered in its timing. A minimum amount of flooding occurs with $c_f = 1.4$. Nonetheless, peak discharge is both delayed and decreased in magnitude. Lowering the flooding criterion to 1.0 and 0.6 achieves the same effect on peak flows but also enhances and delays low flows. A similar effect is shown for experiments involving the flood exchange parameter, r_f. Increasing the proportion of volume change attributable to floodplain inundation dampens and shifts the hydrograph forward in time. Clearly, the model Amazon River is highly sensitive to the effects of floodplain storage. It is a critical component of the river's hydrology.

It has been estimated that there are approximately 100,000 km^2 of Amazonian floodplains [Goulding, 1985], up to 100 km wide [Rzóska, 1978]. On average these are inundated for 6 months each year although a range of 2 to 10 months has been reported depending on topography and river level fluctuations [Melack and Lesack, 1988; Goulding, 1985; Herrera, 1985; Pires and Prance, 1985; Adis, 1984; Junk and Howard-Williams, 1984]. WTM determined a 6- to 7-month floodplain inundation over the central Amazon. Considering the impact of flood exchanges on the discharge of channel water and the fact that floodplain inundation is likely to regulate unique and intense metabolic activity [Richey, 1983; Elder, 1985; Fisher, 1986; Melack and Lesack, 1986; Harriss et al., 1988], a realistic treatment of this effect in regional biogeochemical studies, especially in the context of ongoing land use conversion, is critical.

Future Research Needs

Despite their simplicity, WBM and WTM together can characterize water dynamics over large areas of landscape with high spatial and temporal resolution. Although these results are encouraging, there are numerous opportunities to refine and expand the current effort. For instance, the water balance component would clearly benefit from a more refined treatment of storm flow runoff and water ponding in soils. The transport model could be refined to include more sophisticated flow dynamics and a more realistic assignment of flow and flood parameters over space. The combined WBM / WTM simulation now operates at dynamic steady state and requires reformulation to consider transient phenomena. The impact of important episodic events (for example, the El Niño / Southern Oscillation) on the terrestrial water balance and ecosystem dynamics could then be more effectively evaluated. A real-time model also might more readily be checked against data sets collected for specific times and at finer temporal scales. The major limitation in developing such a model is the lack of input data of sufficient quality, scope and spatial resolution.

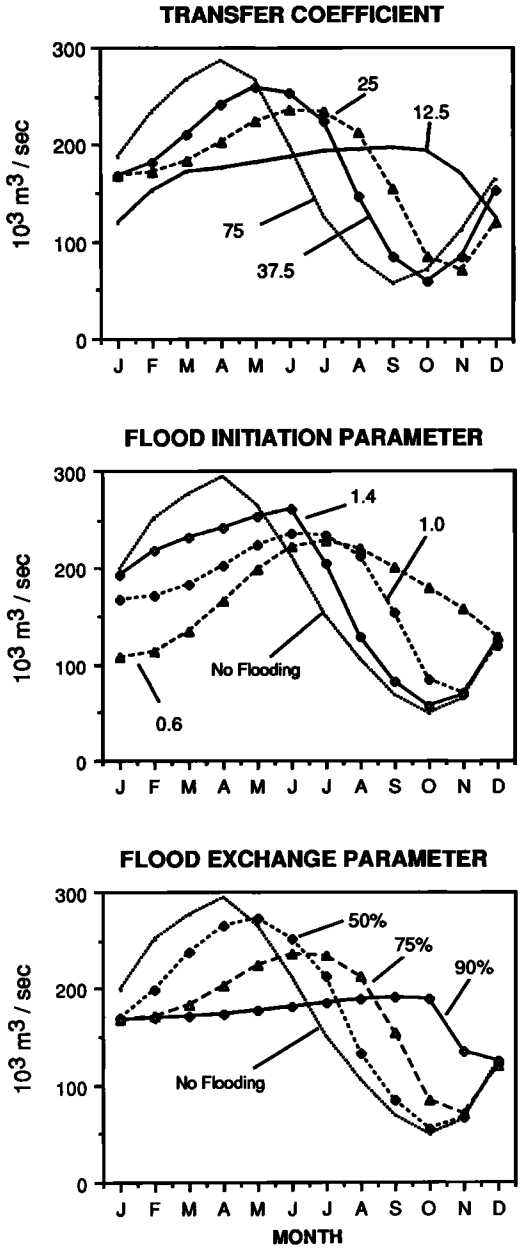

Fig. 15. Model results showing the effect of variation in the fluvial transfer coefficient (K), the flood initiation (c_f), and the flooding exchange parameter (r_f) on the discharge hydrograph at Obidos.

The WBM / WTM is a relatively simple computational device that can be used to study the impact of land use and climate change on surface hydrology and, in turn, terrestrial nutrient cycling and trace gas exchange. We envision an initial series of tests in which we will apply independently derived climate and land cover fields available from maps, digital data sets and / or general circulation model (GCM) studies to explore resultant model behaviors. Since the WBM / WTM is gridded and organized into modules, with suitable refinement it could eventually be incorporated into a GCM context to simulate atmosphere / landscape coupling and quantify more directly the impact of climatic feedbacks on landscape hydrology and nutrient biogeochemistry.

The use of parameters derived from remote sensing in conjunction with models such as WBM / WTM has the potential to provide a comprehensive view of the Earth's hydrology [Johnson, 1986; Goodison, 1985]. For example, use of satellite-borne passive microwave in conjunction with visible and infrared sensors like the advanced very high resolution radiometer (AVHRR) can give an index of vegetation state, soil moisture and water cycling potentials at spatial scales comparable to that used in this study [Tucker et al., 1986; Choudhury, 1988; Choudhury and Golus, 1988]. Active microwave imagery has been used recently to determine the duration and extent of wetland inundation [Imhoff et al., 1987; Hoffer et al., 1986]. High-resolution global data sets for digital topography and channel routing are also feasible using radar altimetry [NASA / Topographic Science Working Group, 1988] and would augment existing global data sets with coarse vertical resolution [NCAR / NAVY, 1984]. The unique and complementary suite of sensors proposed as part of NASA's Earth Observing System (EOS) will provide an unprecedented opportunity to study surface hydrology at the continental scale. Models of continental-scale water balance and transport will be an integral part of this initiative [NASA / EOS, 1984 and supplements].

The hydrologic model reported here will be expanded to include the dynamics of carbon, major nutrients and sediments. It will serve as a semimechanistic tool by which to study the transport of materials from the continents to the world's oceans and help refine current estimates of riverine flux. The model will provide much needed insight into the linkages between climate and fluvial dynamics in large river systems. The enhanced model will provide a mechanism to quantify the impact of climate or land use change on water and material flux in major river systems of the globe.

SUMMARY AND CONCLUSIONS

Water is one of the dominant factors regulating the biogeochemistry of the planet. Gaining an understanding of the linkages between the global hydrologic cycle and the global cycles of carbon, nitrogen and other life-supporting elements is a prerequisite to quantifying the impact of climate and land use change on the Earth's biota. A continental-scale hydrologic model was constructed and applied to South America with emphasis on the Amazonian region. The hydrologic model consists of two components: a water balance model and a water transport model (WBM / WTM). The combined model creates a set of high-resolution data sets for soil moisture, evapotranspiration, runoff, river discharge and floodplain inundation. The work described in this paper is a first step toward eventual global coverage.

The WBM predicts monthly and annual soil moisture, evapotranspiration and runoff for more than 5700 grid cells (1/2° by 1/2°, latitude by longitude) which constitute South America. A set of global data bases covering precipitation, potential ET, temperature, soil texture, vegetation and

topography is used in conjunction with the model to characterize the surface hydrology of diverse landscapes and climate. The data define conditions of long-term, average climate. The WBM calculates the most spatially resolved estimates of terrestrial water cycle components currently available for South America. The distribution and timing of WBM-calculated soil moisture, evapotranspiration and runoff were found to be highly dependent on precipitation. The patterns predicted by the model for the continent compare well with existing data sets, although absolute magnitudes differ, at times substantially [cf. Korzoun et al., 1977; Willmott and Rowe, 1986].

The WTM was applied to the Amazon / Tocantins River system. The model relies on runoff from single grid cells calculated by WBM, river network topology and simultaneous solution of flow and mass balance equations. There are linear transfers of discharge between grid cells and a simple representation of wetland flooding. Scenario experiments using WTM showed that the linear transfer coefficients producing the most reasonable discharge hydrographs were well within the range predicted from geomorphologic principles (average cell turnover of ≈1.5 days). Parameters defining floodplain exchanges which gave the best results also were supported by accounts given in the literature (6-7 months of flooding in the mainstem Amazon). In the model, channel turnover and floodplain inundation combine to produce a pattern in which the upper reaches of the mainstem Amazon are greatly influenced by tributary inputs. In contrast, the lower mainstem river shows propagation of a distinct flood wave and demonstrates a significant capacity to dampen influent signals.

The fluvial discharge and routing components successfully determined the timing and magnitude of discharge for a set of observed hydrographs in the selected basin. Flow at a major downstream site on the Amazon (Obidos) followed the observed interannual pattern, and the calculated annual mean flow was within 1% of observation. Other sites showed disparities from 3 to 33%, with higher values indicating an ill-defined water balance. The record of observed discharge provides an important check against model performance for both fluvial transport and water balance. Unfortunately, the observational data set for the Amazon / Tocantins is sparse. Without a global network of well-instrumented rivers, an accurate geography of the terrestrial water cycle will be difficult to establish.

While our long-term objectives extend beyond the water cycle, hydrologic information is essential for modeling continental- and global-scale distributions of primary production, decomposition, trace gas exchange with the atmosphere and nutrient export to coastal ecosystems. Ultimately, these models will allow us to explore the issue of global change, in terms of both climate and land use. For example, we wish to address questions such as, "What will be the impact of an average 3°C warming on evapotranspiration, river discharge, primary production and trace gas exchanges for the global land mass?" These questions assume growing urgency as sustained increases in atmospheric CO_2, methane and other trace gases foreshadow a global climate well outside the bounds of recent geologic history.

Acknowledgments. The research reported in this paper has involved the efforts of many individuals whom we now recognize. We thank C. Smith and W. Chomentowski for their invaluable assistance in organizing our global data bases and producing usable output. S. Morin carried out and checked the manual routing of our simulated drainage basin. E. Lent organized and carefully entered the tabular data. We also wish to thank C. J. Willmott for his generous assistance in providing global meteorological data sets and for his helpful comments on our work. B. Bergquist, K. Nadelhoffer, and D. Rudnick contributed to early discussions on riverine biogeochemistry. We are grateful to those who reviewed the manuscript and substantially improved upon its content and style: W. B. Bowden, S. L. Dingman, D. Kicklighter, T. Loder, P. Ossenbruggen and J. Raich. Finally, we wish to acknowledge that this research has been supported by the National Aeronautics and Space Administration [grant NAGW-714; contract NA55-30558].

REFERENCES

Adis, J., Seasonal igapó-forests of Central Amazonian blackwater rivers and their terrestrial arthropod fauna, in *The Amazon: Limnology and Landscape Ecology*, edited by Harald Sioli, pp. 245-268, W. Junk, Boston, Mass., 1984.

Akima, H., A method of bivariate interpolation and smooth surface filtering for irregularly-distributed data points, *ACM Trans. Math. Software, 4*(2), 148-159, 1978.

Baumgartner, A., and E. Reichel, *The World Water Balance*, Elsevier, New York, 1975.

Brunskill, G. J., P. Campbell, S. Eliott, B. W. Graham, and G. W. Morden, Rates of transport of total phosphorus and total nitrogen in Mackenzie and Yukon watersheds, NWT and YT, Canada, *Verh. Int. Ver. Theor. Angew. Limnol., 19*, 3199-3203, 1975.

Burges, S. J., Trends and directions in hydrology, *Water Resour. Res., 22*(9), 1S-5S, 1986.

Choudhury, B. J., Relating Nimbus-7 37 GHz data to global land-surface evaporation, primary productivity and the atmospheric CO_2 concentration, *Int. J. Remote Sens., 9*(1), 169-176, 1988.

Choudhury, B. J., and R. E. Golus, Estimating soil wetness using satellite data, *Int. J. Remote Sens., 9*(7), 1251-1257, 1988.

Cluis, D. A., D. Couillard, and L. Potvin, A square grid transport model relating land use exports to nutrient loads in rivers, *Water Resour. Res., 15*(3), 630-636, 1979.

Defense Mapping Agency Aerospace Center, Operational navigation chart M-25, N-25, N-27 and P-28, St. Louis, Mo., 1980.

Defense Mapping Agency Aerospace Center, Operational navigation charts P-26, St. Louis, Mo., 1981.

Defense Mapping Agency Aerospace Center, Operational navigation chart L-27, St. Louis, Mo., 1982.

Defense Mapping Agency Aerospace Center, Operational navigation charts N-26 and P-27, St. Louis, Mo., 1983.

Defense Mapping Agency Aerospace Center, Operational navigation charts L-28, M-26 and M-27, St. Louis, Mo., 1984.

Defense Mapping Agency Aerospace Center, Operational navigation chart L-26, St. Louis, Mo., 1986.

Dickinson, R. E., and A. Henderson-Sellers, Modeling tropical deforestation: A study of GCM land-surface parameterizations, *Q. J. R. Meteorol. Soc.*, *114*, 439-462, 1988.

Dooge, J. C. I., Looking for hydrologic laws, *Water Resour. Res.*, *22*(9), 46S-58S, 1986.

Eagleson, P. S., The emergence of global-scale hydrology, *Water Resour. Res.*, *22*(9), 6S-14S, 1986.

Elder, J. F., Nitrogen and phosphorus speciation and flux in a large Florida river wetland system, *Water Resour. Res.*, *21*(5), 724-732, 1985.

Fearnside, P. M., *Human Carrying Capacity of the Brazilian Rainforest*, Columbia University Press, New York, 1986.

Fisher, T. R., N and P recycling in an Amazon River floodplain lake, paper presented at Symposium on Freshwater Wetlands and Wildlife, sponsored by Univ. of Ga., Savannah River Ecology Laboratory and U. S. Dept. of Energy, Charleston, S. C., 1986.

Food and Agriculture Organization / Complex Systems Research Center, Soil map of the world, 1:5,000,000, 1/2° digitization, UNESCO, Paris, and Univ. of N. H., Durham, 1974.

Food and Agriculture Organization / United Nations Development Program, *Multipurpose survey of the Kafue River Basin: Zambia, vol. III, Climatology and Hydrology*, FAO, Rome, 1968.

Gentry, A. H., and J. Lopez-Parodi, Deforestation and increased flooding of the upper Amazon, *Science*, *210*, 1354-1356, 1980.

Gianessi, L. P., H. M. Peskin, and G. K. Young, Analysis of national water pollution control policies, 1, A national network model, *Water Resour. Res.*, *17*(4), 796-801, 1981.

Goodison, B. E. (Ed.), *Hydrological Applications of Remote Sensing and Remote Data Transmission, IAHS Publ. 145*, 684 pp., International Association of Hydrological Sciences, Wallingford, U. K., 1985.

Goulding, M., Forest fishes of the Amazon, in *Key Environments: Amazonia*, edited by G. T. Prance and T. E. Lovejoy, pp. 267-276, Pergamon, New York, 1985.

Harriss, R. C., S. C. Wofsy, M. Garstang, E. V. Browell, L. C. B. Molion, R. J. McNeal, H. M. Hoell, R. J. Bendura, S. M. Beck, R. L. Navarro, J. T. Riley, and R. L. Snell, The Amazon boundary layer experiment (ABLE 2A), *J. Geophys. Res.*, *93*, 1351-1360, 1988.

Havel, J. J., and K. J. Bligh, Estimation of water yield coefficients, in *On Rational Groups: Systems Analysis in Catchment Land Use Planning*, edited by D. Bennett and J. F. Thomas, pp. 208-221, Amsterdam, 1982.

Herrera, R., Nutrient cycling in Amazonian forests, in *Key Environments: Amazonia*, edited by G. T. Prance and T. E. Lovejoy, pp. 95-108, Pergamon, New York, 1985.

Hoffer, R., D. F. Lozano-Garcia, D. D. Gillespie, P. W. Mueller, and M. J. Ruzek, Analysis of multiple incidence angle SIR-B data for determining forest stand characteristics, paper presented at the 2nd Space-Borne Imaging Radar Symposium, Jet Propul. Lab., Pasadena, Calif., May 1986.

Huggins, L. F., and J. R. Burney, Surface runoff, storage and routing, in *Hydrologic Modeling of Small Watersheds*, edited by C. T. Haan, American Society of Agricultural Engineers, Monogr. *5*, St. Joseph, Mich., 1982.

Imhoff, M. L., C. Vermillion, M. H. Story, A. M. Choudhury, A. Gafoor, and F. Polcyn, Monsoon flood boundary delineation and damage assessment using space borne imaging radar and Landsat data, *Photogramm. Eng. Remote Sens.*, *53*(4), 405-413, 1987.

International Geosphere-Biosphere Program, *Toward an Understanding of Global Change*, 213 pp., National Academy Press, Washington, D.C., 1988.

Johnson, A. I. (Ed.), *Hydrologic Applications of Space Technology, IAHS Publ. 160*, 488 pp. International Association of Hydrological Sciences, Wallingford, U. K., 1986.

Junk, W. J., and C. Howard-Williams, Ecology of aquatic macrophytes in Amazonia, in *The Amazon: Limnology and Landscape Ecology*, edited by Harald Sioli, pp. 269-293, W. Junk, Boston, Mass., 1984.

Kellogg, W. W., and Z. C. Zhao, Sensitivity of soil moisture to doubling of carbon dioxide in climate model experiments, I, North America, *J. Climate*, *1*, 348-356, 1988.

Korzoun, V. I., A. A. Sokolov, M. I. Budyko, K. P. Voskresensky, G. P. Kalinin, A. A. Konoplyantsev, E. S. Korotkevich, and M. I. Lvovich, *Atlas of World Water Balance*, UNESCO, Paris, 1977.

Leopold, L. B., M. G. Wolman, and J. P. Miller, *Fluvial Processes in Geomorphology*, W. H. Freeman, New York, 1964.

Likens, G. E., F. H. Bormann, R. S. Pierce, J. S. Eaton, N. M. Johnson, *Biogeochemistry of a Forested Ecosystem*, 146 pp., Springer-Verlag, New York, 1977.

Matthews, E., Global vegetation and land use: New high resolution data bases for climate studies, *J. Clim. Appl. Meteorol.*, *22*, 474-487, 1983.

Melack, J. M., and L. F. W. Lesack, Inputs of nitrogen and phosphorus to the flood plain of the Amazon River, paper presented at the Symposium on Freshwater Wetlands and Wildlife, sponsored by Univ. of Ga., Savannah River Ecology Laboratory and U. S. Dept. of Energy, Charleston, S. C., 1986.

Melack, J. M., and L. F. W. Lesack, Export of nitrogen and phosphorus from the central Amazon floodplain to the river, paper presented at the Chapman Conference on the Fate of Particulate and Dissolved Components within the Amazon Dispersal System: River and Ocean, American Geophysical Union, Charleston, S. C., 1988.

Meybeck, M., Carbon, nitrogen and phosphorus transport by world rivers, *Am. J. Sci.*, *282*, 401-450, 1982.

Milliman, J. D., and R. H. Meade, World-wide delivery of river sediment to the oceans, *J. Geol.*, *91*(1), 1-21, 1983.

Moore, B., III., M. P. Gildea, C. J. Vorosmarty, D. L. Skole, J. M. Melillo, B. J. Peterson, E. B. Rastetter, and P. A. Steudler, Biogeochemical cycles, in *Global Ecology*, edited by E. Rambler, L. Margulis and D. Sagan, Academic, Boston, Mass., 1989.

National Aeronautics and Space Administration, Earth observing system: Science and mission requirements working group report, vol. 1, Technical Memorandum 86129, 51 pp., NASA, 1984.

National Aeronautics and Space Administration / Earth System Sciences Committee, *Earth System Science: A*

Closer View, 208 pp., NASA, Washington, D. C., 1988.
National Aeronautics and Space Administration / Topographic Science Working Group, Topographic science working group report to the land processes branch, Earth science and applications division, 64 pp., NASA Lunar and Planetary Institute, Houston, Texas, 1988.
National Center for Atmospheric Research / NAVY, Global 10-minute elevation data, digital tape, Natl. Oceanic and Atmos. Admin., Natl. Geophys. Data Center, Boulder, Colo., 1984.
Pastor, J., and W. M. Post, Calculating Thornthwaite and Mather's actual evapotranspiration using an approximating function, *Can. J. For. Res., 14,* 466-467, 1984.
Pires, J. M., and G. T. Prance, The vegetation types of the Brazilian Amazon, in *Key Environments: Amazonia,* edited by G. T. Prance and T. E. Lovejoy, pp.109-145, Pergamon, New York, 1985.
Quay, P. D., S. L. King, J. M. Lansdown, and D. O. Wilbur, Isotopic composition of methane released from wetlands: Implications for the increase in atmospheric methane, *Global Biogeochem. Cycles, 2,* 385-397, 1988.
Richards, K., *Rivers: Form and Process in Alluvial Channels,* Methuen, London, 1982.
Richey, J. E., Interactions of C, N, P, and S in river systems: A biogeochemical model, in *The Major Biogeochemical Cycles and Their Interactions,* edited by B. Bolin, and R. B. Cook, pp. 365-383, John Wiley, New York, 1983.
Richey, J. E., and M. N. G. Ribeiro, Element cycling in the Amazon Basin: A riverine perspective, in *The Geophysiology of Amazonia,* edited by R. Dickinson, pp. 245-250, John Wiley, New York, 1987.
Richey, J. E., R. H. Meade, E. Salati, A. H. Devol, C. F. Nordin, Jr., and U. dos Santos, Water discharge and suspended sediment concentrations in the Amazon River: 1982-1984, *Water Resour. Res., 22*(5), 756-764, 1986.
Rzóska, J., *On the Nature of Rivers, with Case Stories of Nile, Zaire and Amazon,* 67 pp., W. Junk, Boston, Mass., 1978.
Salati, E., The climatology and hydrology of Amazonia, in *Key Environments: Amazonia,* edited by G. T. Prance and T. E. Lovejoy, pp. 18-48, Pergamon, New York, 1985.
Salati, E., and J. Marques, Climatology of the Amazon region, in *The Amazon: Limnology and Landscape Ecology,* edited by Harald Sioli, pp. 85-126, W. Junk, Boston, Mass., 1984.
Salati, E., and P. B. Vose, Amazon Basin: A system in equilibrium, *Science, 225*(4658), 129-225, 1984.
Saxton, K. E., W. J. Rawls, J. W. Romberger, and R. I. Papendick, Estimating generalized soil water characteristics from texture, *Soil Sci. Soc. Am. J., 50*(4), 1031-1036, 1986.
Schmidt, E. J., Water quality impact of non-point source contaminants in small tidal rivers, Ph.D. thesis, Univ. of N. H., Durham, 1981.
Singh, V. P. (Ed.), *Rainfall-Runoff Relationships,* Water Resources Publications, Littleton, Colo., 1982.
Stallard, R., and J. M. Edmond, Geochemistry of the Amazon, 2, The influence of geology and weathering environment on the dissolved load, *J. Geophys. Res., 88,* 9671-9688, 1983.
Thornthwaite, C. W., and J. R. Mather, Instructions and tables for computing potential evapotranspiration and the water balance, *Drexel Inst. Technol. Publ. Clim., X*(3), 1957.
Tucker, C. J., J. R. G. Townshend, and T. Goff, Continental land cover classification using NOAA-7 AVHRR data, *Science, 227,* 369-375, 1986.
UNESCO, *Discharge of Selected Rivers of the World, vol II, Monthly and Annual Discharges Recorded at Various Selected Stations (from start of observations to 1964),* UNESCO, Paris, 1969.
UNESCO, *Discharge of Selected Rivers of the World, vol. III, Mean Monthly and Extreme Discharges, part I, (1965-1969),* UNESCO, Paris, 1971.
UNESCO, *Discharge of Selected Rivers of the World, vol. III, Mean Monthly and Extreme Discharges, part II, (1969-1972),* UNESCO, Paris, 1974.
UNESCO, *Discharge of Selected Rivers of the World, vol. III, Mean Monthly and Extreme Discharges, part III, (1972-1975),* UNESCO, Paris, 1979.
UNESCO, *Discharge of Selected Rivers of the World, vol. III, Mean Monthly and Extreme Discharges, part IV, (1976-1979),* UNESCO, Paris, 1985.
United Nations, *River Inputs to Ocean Systems,* UNIPUB, New York, 1981.
Vorosmarty, C. J., M. P. Gildea, B. Moore, B. J. Peterson, B. Bergquist, and J. M. Melillo, A global model of nutrient cycling, II., Aquatic processing, retention and distribution of nutrients in large drainage basins, in *Watershed Research Perspectives,* edited by D. Correll, pp. 32-56, Smithsonian Institution Press, Washington, D. C., 1986.
Willmott, C. J., Some comments on the evaluation of model performance, *Bull. Am. Meteorol. Soc., 63*(11), 1309-1313, 1982.
Willmott, C. J., and C. M. Rowe, Terrestrial water budget data archive: Version 1.01, Univ. of Del., Dep. of Geog., Newark, 1986.
Willmott, C. J., C. M. Rowe, and Y. Mintz, Climatology of the terrestrial seasonal water cycle, *J. Clim., 5,* 589-606, 1985a.
Willmott, C. J., S. G. Ackleson, R. E. Davis, J. J. Feddema, K. M. Klink, D. R. Legates, J. O'Donnell, and C. M. Rowe, Statistics for the evaluation and comparison of models, *J. Geophys. Res., 90*(C5), 8995-9005, 1985b.
Wiltshire, S. E., D. G. Morris, and M. A. Beran, Digital data capture and automated overlay analysis for basin characteristic calculation, *Cartogr. J., 23,* 60-65, 1986.

M. Patricia Gildea, A. L. Grace, B. Moore III, and C. J. Vorosmarty, Institute for the Study of Earth, Oceans, and Space, University of New Hampshire, Durham, NH 03824.

J. M . Melillo, B. J. Peterson, E. B. Rastetter, and P. A. Steudler, Ecosystems Center, Marine Biological Laboratory, Woods Hole, MA 02543.

(Received April 14, 1989;
revised July 24, 1989;
accepted July 31, 1989.)